Title

The anticancer human mTOR inhibitor sapanisertib potently inhibits multiple Plasmodium kinases and life cycle stages.

Journal

Science Translational Medicine, 14(667)

Authors

Arendse, Lauren

Murithi, James

Qahash, Tarrick

et al.

Publication Date

2022-10-19

DOI

10.1126/scitranslmed.abo7219

Peer reviewed

HHS Public Access

Author manuscript

Sci Transl Med. Author manuscript; available in PMC 2023 October 19.

Published in final edited form as:

Sci Transl Med. 2022 October 19; 14(667): eabo7219. doi:10.1126/scitranslmed.abo7219.

The anticancer human mTOR inhibitor sapanisertib potently inhibits multiple *Plasmodium* kinases and life cycle stages

Lauren B. Arendse[1,2,3], **James M. Murithi**[4], **Tarrick Qahash**[5,6], **Charisse Flerida A. Pasaje**[7], **Luiz C. Godoy**[7], **Sumanta Dey**[7], **Liezl Gibhard**[1], **Sonja Ghidelli-Disse**[8], **Gerard Drewes**[8], **Marcus Bantscheff**[8], **Maria J. Lafuente-Monasterio**[9], **Stephen Fienberg**[1,10], **Lynn Wambua**[2,10], **Samuel Gachuhi**[10], **Dina Coertzen**[11], **Mariëtte van der Watt**[11], **Janette Reader**[11], **Ayesha S. Aswat**[12,13], **Erica Erlank**[12,13], **Nelius Venter**[12,13], **Nimisha Mittal**[14], **Madeline R. Luth**[14], **Sabine Ottilie**[14], **Elizabeth A. Winzeler**[14], **Lizette L. Koekemoer**[12,13], **Lyn-Marie Birkholtz**[11], **Jacquin C. Niles**[7], **Manuel Llinás**[5,6,15], **David A. Fidock**[4,16], **Kelly Chibale**[1,2,3,10,*]

[1]Drug Discovery and Development Centre (H3D), University of Cape Town, Rondebosch, Cape Town 7701, South Africa.

[2]Institute of Infectious Disease and Molecular Medicine, University of Cape Town, Observatory, Cape Town 7925, South Africa.

[3]South African Medical Research Council Drug Discovery and Development Research Unit, University of Cape Town, Rondebosch, Cape Town 7701, South Africa.

[4]Department of Microbiology and Immunology, Columbia University Irving Medical Center, New York, NY 10032, USA.

[5]Department of Biochemistry and Molecular Biology, Pennsylvania State University, University Park, PA 16802, USA.

[6]Huck Center for Malaria Research, Pennsylvania State University, University Park, PA 16802, USA.

[*]Corresponding author: kelly.chibale@uct.ac.za.

Author contributions: N.M. performed ABS and liver stage susceptibility testing. D.C., M.v.d.W., and J.R. performed gametocytocidal, gamete exflagellation inhibition, and female gamete activation assays. E.E., N.V., A.S.A., and L.L.K. performed SMFA analysis and interpretation of data. S.G. synthesized sapanisertib for in vivo NSG mouse studies. L.G. performed NSG mouse studies. S.G.-D., G.D., M.B., and M.J.L.-M. performed chemoproteomic studies. L.B.A. and L.W. performed recombinant kinase inhibition studies. C.F.A.P., L.C.G., and S.D. performed cKD experiments. J.M.M. performed resistance selections. M.R.L. analyzed sequencing data. S.F. performed in silico docking studies. T.Q. carried out all metabolomics experiments. S.O., E.A.W., L.L.K., L.-M.B., J.C.N., M.L., D.A.F., and K.C. supervised individual laboratory efforts and provided expertise. L.B.A. wrote the manuscript with input from K.C., D.A.F., and other authors. All authors approved the final manuscript.

Supplementary Materials
This PDF file includes:
Figs. S1 to S3
Other Supplementary Material for this manuscript includes the following:
Data files S1 to S6
MDAR Reproducibility Checklist

Competing interests: The authors declare that they have no competing interests.

Data and materials availability: All metabolomics data are available publicly through the NCBI Metabolomics Workbench (62) (Project ID: PR001275). All other relevant data are available in the Supplementary Materials. Requests for resources and reagents should be directed to the corresponding author.

[7]Department of Biological Engineering, Massachusetts Institute of Technology, Cambridge, MA 02139, USA.

[8]Cellzome GmbH, a GSK Company, Heidelberg 69117, Germany.

[9]Tres Cantos Medicines Development Campus-Diseases of the Developing World, GlaxoSmithKline, Tres Cantos, Madrid 28760, Spain.

[10]Department of Chemistry, University of Cape Town, Rondebosch, Cape Town 7701, South Africa.

[11]Department of Biochemistry, Genetics and Microbiology, Institute for Sustainable Malaria Control, University of Pretoria, Hatfield 0028, South Africa.

[12]Wits Research Institute for Malaria, School of Pathology, Faculty of Health Sciences, University of the Witwatersrand, Johannesburg 2193, South Africa.

[13]Centre for Emerging Zoonotic and Parasitic Diseases, National Institute for Communicable Diseases of the National Health Laboratory Service, Johannesburg 2193, South Africa.

[14]School of Medicine, University of California, San Diego, La Jolla, CA 92093, USA.

[15]Department of Chemistry, Pennsylvania State University, University Park, PA 16802, USA.

[16]Center for Malaria Therapeutics and Antimicrobial Resistance, Division of Infectious Diseases, Columbia University Irving Medical Center, New York, NY 10032, USA.

Abstract

Compounds acting on multiple targets are critical to combating antimalarial drug resistance. Here, we report that the human “mammalian target of rapamycin” (mTOR) inhibitor sapanisertib has potent prophylactic liver stage activity, in vitro and in vivo asexual blood stage (ABS) activity, and transmission-blocking activity against the protozoan parasite *Plasmodium* spp. Chemoproteomics studies revealed multiple potential *Plasmodium* kinase targets, and potent inhibition of *Plasmodium* phosphatidylinositol 4-kinase type III beta (PI4Kβ) and cyclic guanosine monophosphate–dependent protein kinase (PKG) was confirmed in vitro. Conditional knockdown of PI4Kβ in ABS cultures modulated parasite sensitivity to sapanisertib, and laboratory-generated *P. falciparum* sapanisertib resistance was mediated by mutations in PI4Kβ. Parasite metabolomic perturbation profiles associated with sapanisertib and other known PI4Kβ and/or PKG inhibitors revealed similarities and differences between chemotypes, potentially caused by sapanisertib targeting multiple parasite kinases. The multistage activity of sapanisertib and its in vivo antimalarial efficacy, coupled with potent inhibition of at least two promising drug targets, provides an opportunity to reposition this pyrazolopyrimidine for malaria.

INTRODUCTION

Malaria, a parasitic disease caused by the protozoan *Plasmodium* and transmitted to humans via the female *Anopheles* mosquito vector, remains a serious health problem, particularly in sub-Saharan Africa (1). Malaria disproportionately affects young children and pregnant women, with the *Plasmodium falciparum* (*Pf*) species causing the most severe form of disease. *Plasmodium vivax* (*Pv*) is the other major species responsible for human disease,

and although this species is less lethal than *P. falciparum*, it causes a relapsing form of the disease that poses an additional challenge for malaria control. The emergence of resistance to a range of antimalarials and increasing reports of delayed parasite clearance for first-line artemisinin-based combination therapies are major concerns for managing this global public health issue (2). There is an urgent search for new treatments with alternative modes of action relative to current therapies, offering both curative and transmission-blocking activity (TBA) and having a low risk of resistance (3).

The *Plasmodium* life cycle is complex, offering several opportunities for therapeutic intervention. To aid malaria eradication efforts, chemotherapeutic agents with activity against the parasite's asexual blood stage (ABS) are needed to treat malaria symptoms, and those that target sexual stages to block host-to-vector transmission are also highly desirable. *Plasmodium* kinases have emerged as promising potential drug targets for malaria, with several demonstrating the potential to yield antimalarials with multistage activity (4). The extensive use of human kinase inhibitors for the treatment of cancer and other diseases provides an opportunity to repurpose and reposition chemical matter from these programs for malaria.

Here, we report the antiplasmodial prophylactic liver stage activity, in vitro and in vivo ABS activity, and transmission-blocking activity of the pyrazolopyrimidine human kinase inhibitor sapanisertib (also known as MLN0128, INK128, and TAK-228, Fig. 1A). Sapanisertib is an adenosine triphosphate (ATP)–competitive inhibitor of the "mammalian target of rapamycin" (mTOR) complex 1 and 2 that is under clinical investigation for cancer treatment (5). mTOR is an atypical phosphatidylinositol 3-kinase (PI3K)–related protein kinase, which serves as a key regulator for a wide range of cellular processes, including immune responses and autophagy. However, no clear mTOR orthologs have been identified in *Plasmodium* (6). Using a combination of chemoproteomic tools and biochemical assays using recombinantly expressed kinases, we demonstrate that sapanisertib is a multikinase inhibitor that inhibits *Plasmodium* phosphatidylinositol 4-kinase type III beta (PI4Kβ) and cyclic guanosine monophosphate (cGMP)–dependent protein kinase (PKG), in addition to several other putative targets. Conditional knockdown (cKD) of *Pf*PI4Kβ in ABS parasites resulted in sensitization to sapanisertib, and in vitro *P. falciparum* sapanisertib resistance was mediated through mutations within the ATP-binding site of *Pf*PI4Kβ. These data implicate this essential lipid kinase as the primary target in ABS parasites. Molecular modeling studies revealed key protein-inhibitor interactions in the *Plasmodium* PI4Kβ and PKG ATP-binding sites, providing a starting point for the structure-based repositioning of sapanisertib as a dual kinase inhibitor to treat malaria. Furthermore, a metabolomics study comparing the effect of sapanisertib and other chemically distinct PI4Kβ and/or PKG inhibitors on key *Plasmodium* biochemical pathways revealed some key similarities and differences between chemotypes, with disruption to hemoglobin metabolism being a characteristic feature observed for all PI4Kβ inhibitors tested.

RESULTS

Sapanisertib displays in vitro ABS, prophylactic liver stage, and transmission-blocking antiplasmodial activity

Sapanisertib displayed potent in vitro antiplasmodial activity against ABS parasites, with a 50% inhibitory concentration (IC_{50}) of 76 nM against the multidrug-resistant *Pf*Dd2 line in a 72-hour growth inhibition assay (Fig. 1, B and C). Sapanisertib was also tested for activity against other life cycle stages using a range of in vitro assays. In a liver stage assay using recombinant *Plasmodium berghei* parasites expressing luciferase, sapanisertib inhibited parasite invasion of HepG2 liver cells with an IC_{50} of 134 nM (Fig. 1D). In comparison, sapanisertib displayed low cytotoxicity against HepG2 cells in culture with a 50% cytotoxic concentration (CC_{50}) of 6 μM and a selectivity index (SI) of 45 (Fig. 1B). The potential of sapanisertib to block host-to-vector transmission was assessed using a series of assays involving the sexual stages of the parasite life cycle (Fig. 1, B, E, and F). For in vitro gametocytocidal assays, sapanisertib showed selectivity for late-stage gametocytes, inhibiting the viability of *Pf*NF54 stage IV/V gametocytes with an IC_{50} of 538 nM (Fig. 1E). Minimal activity was observed against early-stage gametocytes (*Pf*NF54 stages II/III; 30% inhibition at 5 μM inhibitor concentration). Sapanisertib also significantly inhibited male and female gamete formation (89 and 97% inhibition at 2 μM inhibitor concentration) in an in vitro exflagellation inhibition assay (EIA) and a female gamete activation assay (FGAA). The transmission-blocking potential of this compound was further demonstrated in a standard membrane feeding assay (SMFA). In the SMFA, sapanisertib was incubated with stage V gametocytes for 48 hours before mosquito feeding. At a concentration of 2 μM, sapanisertib reduced the mean oocyst formation (±SD) in the mosquito midgut by 54% (±23%) and the mean prevalence of infected mosquitoes by 44% (±6%) relative to controls, as measured by the percent transmission-reducing activity (TRA) and TBA, respectively (Fig. 1, B and F).

Sapanisertib clears blood stage parasites in a *P. falciparum* NSG mouse model of infection

The therapeutic efficacy of sapanisertib was assessed in an NSG (NOD-*scid IL-2Rγ*^{null}) mouse model of *P. falciparum* infection. Sapanisertib was administered as a single daily oral dose for four consecutive days, starting on day 3 after infection. Blood parasitemia levels were monitored over the course of treatment (Fig. 1G). Sapanisertib was efficacious against *P. falciparum* with an ED_{90} value (effective dose that reduces parasitemia by 90% compared to the untreated control group) at day 7 of 0.88 mg/kg. Animals in the dosing group of 10 mg/kg both reached a humane end point before day 7 of the study (weight loss ≥ 15%). The whole-blood concentrations of the compound were monitored at various time points after the first dose of compound to assess the exposure levels responsible for the observed reduction in parasitemia. The pharmacokinetic profile and calculated parameters are shown in fig. S1. The AUC_{ED90} value (estimated average exposure in whole blood that is necessary to reduce parasitemia by 90% on day 7 compared to the untreated control group) could not be determined because of the exposure levels of the dosing groups of 0.1 and 0.05 mg/kg being below the lowest limit of quantification (1 ng/ml) (fig. S1). Mean exposure levels for the dosing group of 10 mg/kg remained above the in vitro IC_{50} of sapanisertib against the

*Pf*NF54 strain (0.058 μM/0.018 μg/ml) for 24 hours, whereas exposure levels for 1 and 0.5 mg/kg dropped below this level between 2 and 3 hours after dosing.

Chemoproteomic studies identify PKG, PI4Kβ, and PI3K as putative *Plasmodium* kinase targets

Sapanisertib was profiled against *P. falciparum* kinases from an ABS extract using beads derivatized with sets of broad-spectrum ATP-competitive kinase inhibitors in competitive binding experiments that allowed for an unbiased kinome-wide approach to identify endogenous kinase targets from cell extracts (7). Two kinobead types (Kinobeads and Lipid-Kinobeads) allowed for the profiling of sapanisertib against 54 *P. falciparum* kinases (data file S2), accounting for over half of the predicted *P. falciparum* kinome (8). Data file S2 lists the apparent dissociation constants (K_d^{app}) determined for proteins that showed a dose-dependent reduction in binding to beads in the presence of free sapanisertib in at least two independent experiments (with the exception of PI3K, $N = 1$). The strongest competition was observed for PKG (PF3D7_1436600), PI4Kβ (PF3D7_0509800), and PI3K [also referred to as vacuolar protein sorting 34 (Vps34); PF3D7_0515300], which displayed K_d^{app} values for sapanisertib of ≤50 nM (Fig. 2A and data file S2). Additional kinases with K_d^{app} values of <1 μM included cdc2-related protein kinase 5 (CRK5; PF3D7_0615500), casein kinase 1 (CK1; PF3D7_1136500), and protein kinase 2 (PK2; PF3D7_1238900). The following nonkinases also showed competition with sapanisertib: (i) suppressor of cytokine signaling 2 (SOC2, PF3D7_1227500), which is involved in the regulation of cyclin-dependent kinases and has been reported to form a complex with CRK5 (9), suggesting that sapanisertib interactions with SOC2 are indirect; (ii) γ-glutamylcysteine synthetase (PF3D7_0918900); and (iii) four potential members of the highly conserved kinase, endopeptidase, and other proteins of small size (KEOPS) complex [uncharacterized protein with cancer/testis antigen (CTAG)/Pcc1 domain (PF3D7_0610700), subunit CGI121 (PF3D7_0511700), the transfer RNA N6-adenosine threonylcarbamoyltransferase kidney anion exchanger 1 (kAE1; PF3D7_1030600), and BUD32 (PF3D7_0708300)]. BUD32 is a kinase that is thought to play a supporting role for the catalytic subunit KAE1 within the KEOPS complex.

Biochemical assays confirm potent inhibition of *Plasmodium* PKG and PI4Kβ

In vitro kinase inhibition assays using purified recombinant proteins confirmed the direct interaction of sapanisertib with PKG and PI4Kβ. Sapanisertib inhibited *Pf*PKG with an IC_{50} of 20 nM and *Pv*PI4Kβ with an IC_{50} of 4 nM in the presence of 10 μM ATP (Fig. 2B). *Pf*PI4Kβ and *Pv*PI4Kβ kinase domains share 96% sequence identity, and their ATP-binding sites are predicted to be identical, making *Pv*PI4Kβ a suitable surrogate for *Pf*PI4Kβ (10), which is more challenging to express recombinantly. In vitro inhibition of *Pf*PI3K has previously been reported (IC_{50} = 56 nM) (11), consistent with the Kinobead results.

PI4Kβ knockdown modulates parasite sensitivity to sapanisertib

To validate the role of the top three putative kinase targets from the chemoproteomic studies in the mode of action of sapanisertib, we used *P. falciparum* PKG (12), PI4Kβ, and PI3K

cKD lines to carry out differential susceptibility screening. Using the TetR (Tet repressor protein)/DOZI (development of zygote inhibited)-RNA aptamer module, translation of the target kinase in these parasites is controlled by anhydrotetracycline (aTc), wherein high aTc allows translation, whereas low aTc results in reduced protein expression (13). Knockdown of PI4Kβ caused increased sensitivity to sapanisertib as exhibited by a leftward shift in the dose-response curve and a 10-fold decrease in IC_{50} compared to wild-type levels of expression (Fig. 2C). Evaluation of the knockdown of PKG, PI3K, and an aptamer-regulatable control line did not reveal differential susceptibility to sapanisertib compared to wild-type protein conditions (Fig. 2C). These findings strongly suggest that PI4Kβ is the primary target in *P. falciparum* ABS parasites.

In vitro selections identify resistant mutations in *Pf*PI4Kβ

In vitro resistance selections were carried out to determine possible resistance mechanisms for sapanisertib. Continuous exposure of 10^9 Dd2 parasites (clone Dd2-B2) to sapanisertib at a concentration equal to 5× the 72-hour ABS $IC_{50,}$ in three independent flasks, generated resistant parasites after 16 days. Bulk-resistant cultures displayed sapanisertib IC_{50} values that were 5- and 10-fold higher than the parental line in drug susceptibility assays (Fig. 3A). The resulting sapanisertib-resistant parasites were cloned by limiting dilution to obtain genetically homogeneous cultures. Similarly, the IC_{50} values for phenotyped clones were 7- to 12-fold higher than the parental line (Fig. 3B). Whole-genome sequencing was carried out for six clones, revealing two distinct mutations in the catalytic domain of PI4Kβ (data file S5). Clones from flasks 1 (F1-C01 and F1-C08) and 2 (F2-D02 and F2-F02) had an E1316D mutation, and those from flask 3 (F3-B01 and F3-C05) had the Y1356C mutation (Fig. 3B, right). The E1316D mutation in PI4Kβ conferred higher levels of resistance to sapanisertib compared to the Y1356C mutation.

Molecular modeling studies identify inhibitor-target interactions in the ATP-binding sites of the kinases

In silico molecular docking studies predict that sapanisertib adopts a similar binding pose in the ATP-binding sites of primary and secondary *Plasmodium* kinase targets PI4Kβ and PKG and the human kinase target mTOR (Fig. 4).

In the absence of a structure of *Plasmodium* PI4Kβ, sapanisertib was docked into a homology model of *Pf*PI4Kβ (10) (Fig. 4A). The adenine-like 4-amino-pyrazolopyrimidine core forms typical hinge-binding interactions with the backbone amide of V1357 and carbonyl of E1355 and π-π stacking interactions with F827. The isopropyl group sits in the ribose pocket without clashing with any of the polar residues lining this pocket. The benzoxazole-2-amine extends into the so-called affinity pocket (14) with the oxazole accepting a hydrogen bond from the amine of the conserved catalytic lysine residue (K1308) and backbone amide of D1430 (the aspartate residue forming part of the conserved DFG kinase motif, DYG in *Pf*PI4K), whereas the amine donates a hydrogen bond to the acidic side chains of D1430.

The *Pf*PI4Kβ residues that mutated under drug pressure in vitro to yield sapanisertib-resistant parasites include E1316, a conserved acid found on the αC helix in the catalytic

region of the binding site, and Y1356, a residue located within the hinge that forms aromatic interactions with the adenine-like core of sapanisertib. E1316 is involved in tertiary folding and forms hydrogen bonds with the backbone amides of D1430, Y1431 of the DYG motif, and Y1342 from another loop on the boundary of the active site. The E1316D mutation to a smaller amino acid may reduce the flexibility of the binding site and consequently reduce the favorable binding of the bulky benzoxazole moiety of sapanisertib (Fig. 4C). The Y1356C mutation results in a loss of the aromatic interaction with the adenine-like core of sapanisertib, accounting for the ~7-fold loss in inhibitor potency associated with the parasites containing this mutation.

A crystal structure of *Pv*PKG [Protein Data Bank (PDB) 5F0A] in complex with inhibitor 1FB [1-(tert-butyl)-3-(3-chlorophenoxy)-1H-pyrazolo[3,4-d]pyrimidin-4-amine; fig. S2A] was selected for docking studies, due to the structural similarity between 1FB and sapanisertib. The kinase domains of *Pf*PKG and *Pv*PKG are highly homologous, and the ATP-binding sites are completely conserved (15). In *Pv*PKG, the 4-amino-pyrazolopyrimidine core participates in hydrogen bond interactions with the hinge backbone amide of V614, the backbone carbonyl of E612, and the side chain of T611, the so-called gatekeeper residue (Fig. 4B). However, the sapanisertib core does not form any of the aromatic interactions seen in *Pf*PI4Kβ. The benzoxazole-2-amine extends into the so-called back pocket of *Pv*PKG, a hydrophobic pocket adjacent to the ATP-binding site that is only accessible in protein kinases with a small gatekeeper residue, as is observed in *Plasmodium* PKG (*Pv*PKG T611) (15). The benzoxazole nitrogen accepts a hydrogen bond from the backbone of D675, whereas the amine donates a hydrogen bond to E582 and T586. Again, the isopropyl group sits in the ribose pocket without interacting with any of the polar residues found in this subsite. As expected, the predicted binding pose of sapanisertib is similar to that of inhibitor 1FB cocrystallized in *Pv*PKG.

Sapanisertib docked into human mTOR with a similar pose to the *Plasmodium* kinase targets and the related inhibitor TORkinib (fig. S2B) that was cocrystallized within the human mTOR structure (16) used for these docking studies (Fig. 4C). The 4-amino-pyrazolopyrimidine core of sapanisertib forms hydrogen bonds with the hinge backbone amide and carbonyl of V2240 and G2238, respectively. The benzoxazole-2-amine extends into the affinity pocket, with the oxazole forming hydrogen bonds with D2357 and the catalytic K2187 as observed in *Pf*PI4Kβ. The amine interacts with the D2195 (equivalent to *Pf*PI4K E1316) within the catalytic αC helix and E2190 (equivalent to *Pf*PI4K D1311).

Metabolomic perturbations reveal similarities and differences among polypharmacological kinase inhibitors

An established metabolomics approach (17) was used to assess the impact of sapanisertib on parasite biochemical or metabolic pathways relative to other known *Plasmodium* kinase inhibitors. In each trial, *Pf*3D7 trophozoites were exposed to one of the following inhibitors: sapanisertib, MMV390048, MMV1900328, MMV652103, KAI407, MMV030084, or the control compound atovaquone (Fig. 5). The parasites were treated with 10-fold the IC_{50} value for each of these compounds for 2.5 hours, and the metabolic response to compound exposure was determined by liquid chromatography coupled to mass

spectrometry (LC-MS). An in-depth analysis of the metabolite changes compared to a no-drug control revealed drug-induced disruptions to key metabolic pathways. As previously reported (17), the *Plasmodium* bc1 complex inhibitor atovaquone led to an increase in the pyrimidine biosynthesis precursors dihydroorotate and *N*-carbamoyl-L-aspartate. This metabolic fingerprint is consistent with the disruption of ubiquinone recycling caused by inhibition of the bc1 complex, leading to reduced levels of this cofactor that is required for de novo pyrimidine synthesis. Sapanisertib, MMV390048, MMV1900328 (18), MMV652103, and KAI407 all led to a disruption and reduction of hemoglobin-derived peptides (Fig. 5 and fig. S3). These compounds all target *Pf*PI4Kβ; however, some have also been tested for possible polypharmacological interactions. Sapanisertib and MMV390048 with reported in vitro activity against both *Pf*PI4Kβ and *Pf*PI3K (11, 19) had a relative reduction in hemoglobin-derived peptides that exceeded that observed for the other *Pf*PI4Kβ inhibitors. Sapanisertib also resulted in a more pronounced reduction in the pyrimidine biosynthesis precursors dihydroorotate and *N*-carbamoyl-L-aspartate than the other kinase inhibitors. MMV030084, a *Pf*PKG inhibitor that affects the nonmetabolic process of parasite invasion and egress from the host red blood cell (RBC), did not exhibit significant decreases in hemoglobin-derived peptide levels. Instead, minor increases in most of the metabolites were measured, indicating a global effect on parasite development (12). Sapanisertib also inhibits *Pf*PKG in addition to *Pf*PI4Kβ and *Pf*PI3K but displayed no notable difference in measured peptide abundances relative to MMV390048. KAI407, MMV652103, and MMV1900328 all demonstrated comparable decreases in peptide abundance (Fig. 5B). Although MMV652103, similar to sapanisertib, exhibits activity against *Pf*PKG in vitro (20), this effect is superseded by the *Pf*PI4Kβ targeting and therefore does not have a notable effect on the differences in hemoglobin-derived peptide disruptions (Fig. 5B).

DISCUSSION

Here, we report the potent multistage antiplasmodial activity of the human mTOR inhibitor sapanisertib. Furthermore, we identify its kinase targets in *Plasmodium*, validating PI4Kβ as the primary mode of action in ABS parasites. Consistent with previous reports on the activity of *Plasmodium* PI4Kβ inhibitors across the life cycle (21–23), sapanisertib displayed prophylactic liver stage activity, ABS activity, and TBA, with selectivity toward late-stage gametocytes, in experimental models. Proof of concept was demonstrated in an NSG-humanized mouse model of *P. falciparum* infection wherein sapanisertib displayed an ED_{90} of 0.88 mg/kg, but significant weight loss was observed for animals in the highest dosing group (10 mg/kg), suggesting a narrow therapeutic window. Given the presence of an adenosine-like hinge-binding motif typical of small-molecule ATP-competitive inhibitors, we used a nonbiased kinome-wide chemoproteomic approach using Kinobead technology to identify putative kinase targets from ABS parasite extracts. Several kinases were identified as putative targets in this study, with *Pf*PKG and *Pf*PI4Kβ consistently displaying the highest apparent binding affinity for sapanisertib in multiple independent Kinobead and/or Lipid-Kinobead experiments. A second phosphoinositide kinase, *Pf*PI3K, was also identified as a potential kinase target of sapanisertib, displaying a K_d^{app} of 50 nM, although PI3K was only identified as a putative target in one of the three independently repeated Lipid-Kinobead experiments. In vitro kinase assays using recombinantly expressed protein

confirmed that sapanisertib interacts directly with both *Pf*PKG and *Pv*PI4Kβ potently inhibiting kinase activity with IC_{50} values of 20 and 4 nM, respectively. Although direct interaction with *Pf*PI3K was not confirmed in this study, sapanisertib has previously been reported to inhibit recombinant *Pf*PI3K in vitro with an IC_{50} of 56 nM in an enzyme-linked immunosorbent assay (11), consistent with the Kinobead data reported here.

With no clear mTOR orthologs in *Plasmodium* (6), the closest related proteins to mTOR in *Plasmodium* are the lipid phosphoinositide kinases. Phosphoinositide kinases are responsible for the highly regulated generation of lipid phosphoinositides, which serve as signaling molecules playing a key role in a vast range of cellular functions (24). There are seven putative phosphoinositide kinases in *Plasmodium* (4, 6). These include a single PI3K (most closely resembling the class III PI3K, Vps34) and two PI4Ks (PI4Kα and PI4Kβ most closely resembling type III α and type III β PI4Ks, respectively) that are thought to be essential for ABS development (25). PI4Kβ has been well characterized as a *Plasmodium* target (21–23, 26), and several distinct chemotypes that potently inhibit *Plasmodium* PI4Kβ have been reported, with the most advanced inhibitor progressing to phase 2 clinical studies for the treatment of malaria (21, 27). *Plasmodium* PI3K, thought to play a role in hemoglobin trafficking and autophagy regulation (28, 29), has also been proposed as a potential antimalarial drug target. Although compounds with antiplasmodial activity have been reported to inhibit *Pf*PI3K in vitro (11, 28, 30–32), the selectivity of these compounds is unclear, and other targets may contribute to their whole-cell antiplasmodial activity. The mTOR inhibitor Torin-2 was reported to be highly potent and selective for *Pf*PI3K (IC_{50} = 0.6 nM) relative to *Pf*PI4Kβ in vitro (19). Despite this, a more recent study demonstrated that PI4Kβ is the primary target and resistance mediator of Torin-2 and Torin-2 derivative NCATS-SM3710 in ABS parasites (22). In addition, MMV390048 has also subsequently been reported to potently inhibit *Pf*PI3K in vitro (19), but the implications of this in the cellular environment or the contribution of *Pf*PI3K inhibition to the observed multistage antiplasmodial activity of MMV390048 are unclear.

Plasmodium PKG, a serine/threonine protein kinase displaying striking divergence from human orthologs PRKG1 and PRKG2, has been validated phenotypically and in vivo as a target with the potential to yield antimalarials with multistage activity (33, 34). Studies have demonstrated that potent inhibition of this enzyme using ATP-competitive small-molecule inhibitors disrupts liver cell invasion by sporozoites, merozoite egress from ABS schizonts, and male gamete development (12). Unlike *Pf*PI4Kβ inhibitors that readily yield resistance-mediating mutations in the target *pfpi4kβ* gene in vitro, selections with *Pf*PKG inhibitors ML10 and MMV030084 did not yield mutations in *pfpkg*, despite chemogenetics approaches confirming *Pf*PKG as the primary target (12, 34). Specific *Pf*PKG inhibitors are characterized by a slow in vitro rate of kill and a narrow stage-specific window of activity against ABS parasites (33–35). Despite this, *Plasmodium* PKG is considered a promising target because of its apparent low propensity for resistance, the presence of a small gatekeeper residue allowing inhibitors access to the back pocket that can be exploited for selectivity, and the availability of high-resolution structures for structure-based drug design (15, 34).

Similar to sapanisertib, imidazopyridazines displaying potent antiplasmodial activity and *Plasmodium* PI4K inhibition have also been reported to inhibit *Pf*PKG (20), suggesting that despite significant divergence between protein kinases and phosphoinositide kinases, features within the ATP-binding site of these two targets make them amenable to the design of dual inhibitors. In phosphoinositide kinases, the affinity pocket (14), as the name suggests, plays a key role in inhibitor binding as is observed for sapanisertib docked into the active site of the *Pf*PI4K homology model, with the benzoxazole-2-amine occupying the affinity pocket. This pocket is located in a similar position to the accessible back pocket in *Pf*PKG, allowing inhibitors to bind to both targets in a similar way. cKD studies showed that knockdown of *Pf*PI4Kβ modulated sensitivity to sapanisertib, whereas knockdown of *Pf*PKG and *Pf*PI3K had no significant effect, identifying PI4Kβ as the primary driver for the ABS antiplasmodial activity. This was further supported by the identification of nonsynonymous single-nucleotide polymorphisms (SNPs) mapping to the ATP-binding site of *Pf*PI4K*β* after whole-genome sequencing of drug-resistant clones isolated from *P. falciparum* ABS parasites selected in vitro. Other reported *Pf*PI4K inhibitors have also readily led to *Pf*PI4Kβ-mediated resistance in vitro resulting from copy number variations and/or SNPs in the target gene (21–23, 26, 36). It is worth noting that sapanisertib did not display reduced susceptibility to a MMV390048-resistant line (21) harboring a *Pf*PI4Kβ-A1319V mutation in a cross-resistance screen, highlighting the importance of using multiple *Pf*PI4Kβ-resistant lines when using cross-resistance studies to aid target identification. Furthermore, a study assessing the impact of sapanisertib on parasite biochemical pathways revealed effects on hemoglobin metabolism, a characteristic feature of *Pf*PI4Kβ inhibitors. Despite distinct similarities, a comparison of the metabolic profile for sapanisertib with the profiles generated for other *Pf*PI4Kβ inhibitors revealed distinct differences in the extent to which hemoglobin-derived peptide levels were reduced, which may be attributed to the inhibition of *Pf*PI3K as a secondary/additional target for some inhibitors.

In summary, this study not only identifies a potential strategy for targeting *Pf*PI4Kβ but also opens new avenues for the development of dual *Plasmodium* PI4Kβ and PKG inhibitors. Targeting multiple essential kinases may reduce the likelihood of resistance emerging and the required dose for efficacy (4). Furthermore, targeting multiple kinases with a small molecule has the potential to minimize the pill burden and cost associated with the development of combination drug regimens based on the selection of mechanistically distinct combination partners. *Pf*PI4Kβ, for which rapid parasite clearance has been observed in the clinic, and *Pf*PKG, shown to result in slow parasite death in vitro and predicted to have a low propensity for resistance, provide a compelling target combination for drug development. Obtaining selectivity for *Plasmodium* kinases over host kinases may pose a notable challenge for optimization. mTOR is expressed in both liver cells and RBCs, regulating hepatic lipid metabolism (37) and RBC growth and proliferation. mTOR inhibition has been associated with hematological adverse effects (38). However, it is worth noting that targeting human mTOR complex 1 has been proposed as an adjunctive host-directed therapy for cerebral malaria aimed at modulating the host immune response (39). Understanding the pharmacokinetic/pharmacodynamic drivers of efficacy and the corresponding dosing requirements and therapeutic window for malaria, which may differ

from indications in oncology, will be crucial for future optimization and development of this compound.

MATERIALS AND METHODS

Study design

Phenotypic screening was carried out to identify advanced human kinase inhibitors with potent ABS antiplasmodial activity as potential *Plasmodium* kinase inhibitors for repurposing/repositioning for malaria. After the identification of sapanisertib, extensive profiling was carried out to characterize its antiplasmodial activity across the parasite life cycle. Prophylactic liver, ABS, and transmission-blocking antiplasmodial properties were tested using a range of experimental models, and in vivo blood stage efficacy was assessed in a humanized mouse model of *P. falciparum* infection. Target identification and validation were carried out using chemoproteomic and chemogenetic approaches. In vitro functional kinase assays were used to confirm direct inhibition of putative kinase targets, and molecular modeling was used to identify inhibitor interactions within the kinase ATP-binding sites. In vitro resistance selections were conducted to identify potential resistance mechanisms, and metabolomics profiling was used to assess the impact of sapanisertib on key parasite biochemical pathways.

Chemistry

Sapanisertib was synthesized on the basis of previously described methods (40).

In vitro ABS antiplasmodial assays

In vitro *Pf*Dd2 ABS parasite growth inhibition was determined after 72-hours using the SYBR green assay as previously described (12).

P. berghei liver stage assay

To test for the liver stage activity of sapanisertib, 3000 HepG2-A16-CD81 cells per well were seeded in 1536-well plates (Greiner Bio). Fifty nanoliters of the test and control compound diluted in dimethyl sulfoxide (DMSO) was added and incubated for 24 hours. Thereafter, *P. berghei* sporozoites (*P. berghei* ANKA GFP-Luc-SMcon), freshly obtained by dissecting salivary glands of infected female *Anopheles stephensi* mosquitoes, were added to each well at a density of 1×10^3 per well. The plates were centrifuged for 5 min at 330*g* and incubated at 37°C. Forty-eight hours after infection, 2 μl of luciferin reagent (Promega BrightGlo) was added to each well, and luciferase activity was detected using a PerkinElmer Envision plate reader. IC_{50} values were determined using GraphPad Prism normalized to maximum and minimum inhibition levels for the positive (atovaquone, 0.25 μM) and negative (DMSO) control wells. The in vitro cytotoxicity of sapanisertib against HepG2-A16-CD81 cells was determined in parallel using a CellTitre-Glo (Promega) cell viability assay. Puromycin was used as a positive control (IC_{50} = 0.588 ± 0.003 μM).

In vitro gametocytocidal assays

Stage-specific gametocytocidal action of sapanisertib was determined using an early- and late-gametocyte marker *P. falciparum* cell line, NF54-*pfs*16-GFP-Luc, as previously described (41). Briefly, assays were set up on day 5 (>95% stage II/III gametocytes) and day 10 (>90% stage IV/V gametocytes) using a 2 to 3% gametocytemia and 1.5% hematocrit culture. Gametocytes were incubated for 48 hours under drug pressure in a gas chamber (90% N_2, 5% O_2, and 5% CO_2) at 37°C. A luciferase reporter assay was used to determine IC_{50} values based on three independent biological repeats ($N = 3$) each performed in technical triplicates.

Male gamete EIA

Exflagellation inhibition was measured by capturing the movement of exflagellation centers through time-lapse video microscopy, as previously described (42). Briefly, mature gametocytes (>95% stage V) were treated with 2 μM sapanisertib. After a 48-hour treatment, a 1-ml aliquot was pelleted and resuspended in 50 μl of ookinete medium [RPMI 1640 media containing L-glutamine (Gibco), 202 μM hypoxanthine (Sigma-Aldrich), 0.2% glucose (Sigma-Aldrich), and 0.5% AlbuMAX II (Invitrogen), supplemented with 100 μM xanthurenic acid and 50% (v/v) human serum]. Cultures (10 μl) were transferred to a Neubauer chamber for visualization, and exflagellating centers were recorded by video microscopy (Carl Zeiss NT 6V/10W Stab microscope fitted with a MicroCapture camera, at ×10 magnification). Exflagellating centers were semi-automatically quantified from 16 videos (8 to 10 s each), captured between 16 to 24 min after gametogenesis induction. Videos were analyzed using Icy bio-image analysis software.

Female gamete activation assay

Sapanisertib was evaluated for its ability to inhibit female gamete activation. Gametocytes (>95% stage V) were treated with compound (2 μM) for 48 hours before triggering gamete formation. Female gamete activation was induced by both a temperature drop and the addition of 100 μM xanthurenic acid to ookinete medium. Monoclonal anti-Pfs25 (BEI Resources catalog number MRA-28; 1:1000 dilution) conjugated to fluorescein isothiocyanate was used to detect female gametes. Image acquisition was performed using a Zeiss Axio Lab.A1 epifluorescence microscope with a 100/1.4 numerical aperture oil immersion objective and a Zeiss Axiocam 202 mono digital camera. Using a 100× objective, 30 images were taken per sample and analyzed manually. The size, roundness, and intensity of fluorescence of female gametes were evaluated.

Standard membrane feeding assay

The SMFA was carried out using *Anopheles gambiae s.s.* females (colonized in 2009 from the Democractic Republic of the Congo). The mosquitoes were maintained under biosafety level 2 insectary conditions (80% humidity, 25°C, 12-hour day/12-hour night cycle with 45-min dusk/dawn transitions) (43) with ad libitum access to 10% sucrose supplemented with 0.05% (v/v) 4-aminobenzoic acid. Mature *Pf*NF54 gametocytes (>98% stage V, 1.5 to 2.5% gametocytemia, and 50% hematocrit) were treated with 2 μM sapanisertib with DMSO as a vehicle control for 48 hours before mosquito feeding. SMFA was carried out as

previously described (42). Four independent biological experiments were carried out (total of 71 mosquitoes in treated groups and 69 mosquitoes in control groups). The TRA (Eq. 1), which measures the reduction in oocyst count, and the TBA (Eq. 2), which measures the reduction in prevalence of mosquitoes infected with oocysts, were determined. Data were analyzed using GraphPad Prism, and the Mann-Whitney test was used to compare the statistical significance between the different treatment and control groups.

$$\%\mathrm{TRA} = \frac{Ci - Ti}{Ci} \times 100 \quad (1)$$

$$\%\mathrm{TRA} = \frac{Cp - Tp}{Cp} \times 100 \quad (2)$$

where i is mean oocyst count per mosquito midgut (intensity), p is prevalence of mosquitoes infected with oocysts, C is control groups, and T is treated groups.

P. falciparum NSG mouse model of infection

Efficacy study—The therapeutic efficacy of sapanisertib was evaluated in a murine model of *P. falciparum* infection (44) using a "4-day test." Briefly, NSG mice (male, 6 to 8 weeks old) engrafted with human erythrocytes (about 60%) were infected with 2×10^7 *Pf*3D7-infected erythrocytes from a donor mouse (*P. falciparum* strain *Pf*3D7$^{0087/N9}$, generated in GSK, Tres Cantos, Spain). Infections were done via intravenous injection (day 0). Treatment commenced on day 3 and ended on day 7 after infection. In all cases, parasitemia was assessed in samples of peripheral blood obtained on days 3 to 7 after infection. Fresh samples of peripheral blood from *P. falciparum*–infected mice were stained with TER-119-PE (marker for murine erythrocytes; Biocom Africa, catalog number 116208) and SYTO-16 (nucleic acid dye) and then analyzed via flow cytometry.

Pharmacokinetic analysis—The whole-blood concentrations of sapanisertib were determined using a quantitative LC-MS/MS (tandem MS) method. Sample preparation was achieved with a protein precipitation extraction method, using 10 μl of whole blood and 100 μl of ACN containing the internal standard MMV394902, 5-(4-methylsulfonylphenyl)-3-[4-(trifluoromethyl)phenyl]pyridin-2-amine. The experimental data were evaluated in terms of drug concentration versus time. Noncompartmental analysis was used to calculate the pharmacokinetic parameters of sapanisertib.

All studies and procedures were conducted with prior approval of the animal ethics committee of the University of Cape Town (approval numbers 017/025) in accordance with the South African National Standard (SANS 10386:008) for the Care and Use of Animals for Scientific Purposes (45) and guidelines from the Department of Health (46).

Chemoproteomics

The chemoproteomic affinity capturing experiments were performed as described previously (47) using Kinobeads and Lipid-Kinobeads (7, 48). Kinobeads are a set of promiscuous kinase inhibitors immobilized on Sepharose beads. Briefly, beads were washed and equilibrated in lysis buffer [50 mM tris-HCl (pH 7.4), 0.4% Igepal-CA630, 1.5 mM $MgCl_2$,

5% glycerol, 150 mM NaCl, 25 mM NaF, 1 mM Na_3VO_4, 1 mM dithiothreitol (DTT), and one complete EDTA-free protease inhibitor tablet (Roche) per 25 ml]. The beads were incubated at 4°C for 1 hour with 0.1 ml (0.3 mg) of *Pf*3D7 blood stage extract, which was preincubated with compound or DMSO (vehicle control). The *P. falciparum* blood stage protein extracts were generated as described (21). The experimental set up was such that 10 samples were measured in parallel [TMT 10-plex; (49)] to generate values for the affinity of the beads to the bound proteins ("depletion" values, 4 samples) and to generate IC_{50} values (6 samples) in a single experiment. Samples 1 and 2 were the vehicle control; samples 3 and 4 were done in the same way, except that while the beads were discarded after the first incubation step, the extract was incubated with fresh beads to measure how much protein could rebind to the fresh beads (depleted from the extract by first bead binding). Apparent dissociation constants were determined by taking into account the protein depletion by the beads (48). Samples 5 to 10 were used to generate IC_{50} values by adding compound over a range of concentrations (20 μM, 1:4 and 1:5 dilutions). Beads were transferred to filter plates [Durapore (polyvinylidene difluoride membrane, Merck Millipore)], washed extensively with lysis buffer, and eluted with SDS sample buffer.

Proteins were digested according to a modified single-pot solid-phase sample preparation (SP3) protocol (50). Peptides were labeled with isobaric mass tags (TMT10, Thermo Fisher Scientific, Waltham, MA) using the 10-plex TMT reagents, enabling relative quantification of 10 conditions in a single experiment (49). The labeling reaction was performed in 40 mM triethylammoniumbicarbonate (pH 8.5) at 22°C and quenched with glycine. Labeled peptide extracts were combined to a single sample per experiment, lyophilized, and subjected to LC-MS analysis as described (47). LC-MS/MS measurements on Q Exactive Orbitrap or Orbitrap Fusion Lumos mass spectrometers (Thermo Fisher Scientific) were performed as described (51).

Mascot 2.4 (Matrix Science, Boston, MA) was used for protein identification by using a 10–parts per million mass tolerance for peptide precursors and 20 mD (Higher-energy C-trap dissociation, HCD) mass tolerance for fragment ions. To create the fasta file for mascot searching, all proteins corresponding to the taxonomy "*Plasmodium falciparum* (isolate 3D7)" were downloaded from Uniprot (release 20170621) and supplemented with common contaminant protein sequences of bovine serum albumin (BSA), porcine trypsin, and mouse, rat, sheep, and dog keratins. To assess the false discovery rate (FDR), "decoy" proteins (reverse of all protein sequences) were created and added to the database, resulting in a total of 14,266 protein sequences, 50% forward and 50% reverse.

Unless stated otherwise, we accepted protein identifications as follows: (i) For single-spectrum to sequence assignments, we required this assignment to be the best match and a minimum Mascot score of 31 and a 10× difference of this assignment over the next best assignment. On the basis of these criteria, the decoy search results indicated <1% FDR. (ii) For multiple spectrum to sequence assignments and using the same parameters, the decoy search results indicated <0.1% FDR. Quantified proteins were required to contain at least two unique peptide matches. FDR for quantified proteins was <0.1%. Raw data tables for the chemoproteomics experiments can be found in data file S2.

In vitro *Pf*PKG inhibition assays

Full-length *Pf*PKG (PF3D7_1436600) was expressed in *Escherichia coli* Rosetta 2 (Novagen, EMD_BIO-71402) as previously described (34). Briefly, the N-terminal His-tagged recombinant *Pf*PKG protein was purified using a HisTrap HP column (GE Healthcare), followed by anion exchange and size exclusion chromatography (HiLoad 16/600 Superdex 200-pg column, GE Healthcare). Final buffer composition of purified protein was 50 mM tris-HCl (pH 8.0), 150 mM NaCl, 10 mM β-mercaptoethanol, and 10% glycerol.

*Pf*PKG IC_{50} assays were performed on the basis of previously described methods using the ADP-Glo Kinase Assay (Promega) to measure adenosine diphosphate (ADP) formation (20, 52). Briefly, a threefold serial dilution of each inhibitor was carried out in DMSO, and inhibitors were subsequently diluted into assay buffer [25 mM Hepes (pH 7.4), BSA (0.1 mg/ml), 0.01% (v/v) Triton X-100, 20 mM $MgCl_2$, 2 mM DTT, and 10 μM cGMP] to 1.5× the final required concentration. Two microliters of each inhibitor dilution was transferred into a white 384-shallow well plate (Nunc #264706). A MANTIS Liquid Handler (Formulatrix) was used to dispense the remaining assay components. *Pf*PKG protein (0.5 μl), followed by 0.5 μl of substrate buffer (ATP and peptide substrate GRTGRRNSI-NH2), was added to each well. The final 3 μl of kinase reaction contained 0.6 nM *Pf*PKG protein, 10 μM ATP, 20 μM GRTGRRNSI-NH2, 1% (v/v) DMSO, and inhibitor in assay buffer. Reactions were incubated for 45 min at 22°C (resulting in <10% ATP conversion). ADP formation was measured using the ADP-Glo Kinase Kit (Promega). Briefly, 2 μl of ADP-Glo reagent was added to each well and incubated for 40 min at 22°C to deplete the remaining ATP. Two microliters of kinase detection reagent was then added, and the reaction was incubated for a further 30 minutes at 22°C. The plate was sealed with an adhesive foil seal for all incubation steps. Luminescent signal was measured using the EnSpire Multimode Plate Reader (PerkinElmer). The data were normalized on the basis of the 100% activity controls (1% DMSO only) and the 100% inhibition controls {10 μM *Pf*PKG inhibitor ML10 (*N*-[5-[3-[2-(cyclopropylmethylamino)pyrimidin-4-yl]-7-[(dimethylamino)methyl]-6-methylimidazo[1,2-a]pyridin-2-yl]-2-fluorophenyl]methanesulfonamide; LifeArc}. Mean IC_{50} values were calculated from $n \geq 3$ independent experiments, each with technical duplicates [log(inhibitor) versus normalized response − variable slope].

In vitro *Pv*PI4Kβ inhibition assays

Full-length *Pv*PI4Kβ (PVX_098050) recombinant protein was expressed in a baculovirus-insect cell expression system and purified as previously described (20, 23). Briefly, N-terminal His-tagged recombinant *Pv*PI4Kβ protein was purified using a HisTrap HP column (GE Healthcare), followed by size exclusion chromatography (HiLoad 16/600 Superdex 200 pg column, GE Healthcare). Final buffer composition of purified protein was 20 mM Hepes (pH 7.5), 500 mM NaCl, 5% (v/v) glycerol, and 10 mM β-mercaptoethanol.

*Pv*PI4Kβ kinase inhibition assays were performed using the ADP-Glo kinase assay kit (Promega) to measure ADP formation. L-α-phosphatidylinositol (PI; Avanti Polar Lipid, catalog number 840042P) dissolved in 3% *n*-octylglucoside to a stock concentration of 20 mg/ml was used as the lipid substrate. Briefly, a threefold serial dilution of each

inhibitor was carried out in DMSO, and inhibitors were subsequently diluted into assay buffer [25 mM Hepes (pH 7.4), 100 mM NaCl, 3 mM $MgCl_2$, 1 mM DTT, and BSA (0.025 mg/ml), and 0.2% (v/v) Triton X-100] to 1.5× the final required concentration. Two microliters of each inhibitor dilution was transferred into a white 384-shallow well plate (Nunc #264706). A MANTIS Liquid Handler (Formulatrix) was used to dispense the remaining assay components. *Pv*PI4Kβ protein (0.5 μl) followed by 0.5 μl of substrate buffer (ATP and PI) was added to each well. The final 3 μl of kinase reaction contains ~6 nM *Pv*PI4Kβ protein, 10 μM ATP, PI (0.1 mg/ml), 1% (v/v) DMSO, and inhibitor in assay buffer. Reactions were incubated for 45 min at 22°C (resulting in <10% ATP conversion). ADP formation was measured using the ADP-Glo Kinase Kit (Promega) as described for *Pf*PKG, the only difference being that 10 mM $MgCl_2$ was added to the ADP-Glo reagent prior to use. *Pv*PI4Kβ inhibitor MMV390048 at 10 μM was used as the control (100% inhibition), and data were analyzed as described for *Pf*PKG.

Compound susceptibility assays using *P. falciparum* kinase cKD lines

A stock solution of sapanisertib was serially diluted to yield final concentrations ranging from 1 to 500 nM in the assay. Synchronous ring-stage PKG (PF3D7_1436600) (12), PI4Kβ (PF3D7_0509800), and PI3K (PF3D7_0515300) cKD parasite lines, as well as a control cell line expressing an aptamer-regulatable fluorescent protein, were maintained in the presence of high aTc (500 nM) or low aTc (2 nM in the case of PKG and no aTc in the case of PI4Kβ and PI3K) and distributed into 384-well polystyrene microplates (Corning). Compounds were transferred to the parasite-containing plates using the Janus platform (PerkinElmer). DMSO and dihydroartemisinin treatment (500 nM) served as reference controls. Luminescence was measured after 72 hours using the *Renilla*-Glo Luciferase Assay System (Promega E2750) and the GloMax Discover Multimode Microplate Reader (Promega), and IC_{50} values were obtained from corrected dose-response curves using Graph-Pad Prism.

In vitro selections for sapanisertib resistance

Drug stocks were made at 10 mM in DMSO. All in vitro studies were done such that the final DMSO concentration was <0.5%. The *P. falciparum* ABS parasites used in this study were cultured at 3% hematocrit in human O^+ RBCs in RPMI 1640 media, supplemented with 25 mM Hepes, hypoxanthine (50 mg/liter), 2 mM L-glutamine, 0.225% sodium bicarbonate, 0.5% (w/v) AlbuMAX II (Invitrogen), and gentamycin (10 μg/ml), in modular incubator chambers (Billups-Rothenberg) at 5% O_2, 5% CO_2, and 90% N_2 at 37°C. The *Pf*Dd2-B2 line was cloned by limiting dilution from Dd2 (a gift from T. Wellems, National Institute of Allergy and Infectious Diseases, National Institutes of Health, Rockville, MD). Selections were initiated by exposing three independent flasks, each containing 10^9 wild-type Dd2-B2 ABS parasites to 260 nM sapanisertib, which is 5× the 72-hour ABS IC_{50}. Medium containing sapanisertib was refreshed daily until sensitive parasites were effectively cleared, after which the medium was refreshed every other day, and the culture volume reduced gradually. The resulting sapanisertib-resistant parasites (obtained after 16 days) were cloned by limiting dilution as previously described (34) to obtain genetically homogeneous cultures for further phenotyping and whole-genome sequencing. Drug susceptibility of resistant bulk and clonal lines was assessed by exposing

unsynchronized parasites for 72 hours to 10 different concentrations of sapanisertib, plus control no-drug conditions, starting with predominantly rings (53).

Whole-genome sequencing of sapanisertib-resistant parasites

DNA from sapanisertib-resistant parasites was extracted using the QiAmp DNA Blood Mini Kit (Qiagen) and subjected to whole-genome sequencing using short-read technology. Sample libraries were prepared with the Illumina Nextera XT Kit and sequenced on a NovaSeq 6000 to obtain 100-bp paired-end reads. Reads were aligned to the *Pf* parental genome (PlasmoDB version 36) using the BWA-mem algorithm (Burrows-Wheeler Aligner). Unmapped reads and polymerase chain reaction duplicates were removed using Samtools and Picard. The reads were realigned around indels using Genome Analysis Toolkit (GATK) Realigner-TargetCreator and IndelRealigner, and base quality scores were recalibrated using GATK BaseRecalibrator. GATK HaplotypeCaller (version 3.5) was used to call variants in clones, and variants were subsequently filtered on the basis of quality scores (variant quality as function of quality of depth (QD) > 2, mapping quality > 40, and read depth (DP) > 7). High-quality SNPs were annotated using SnpEFF (54). The list of variants from resistant clones was compared against the *Pf*Dd2-B2 parental clone to obtain homozygous SNPs present exclusively in the resistant clones. Integrated Genome Viewer was used to confirm polymorphisms present in resistant clones.

In silico molecular docking

The *Pf*PI4Kβ homology model (10), the *Pv*PKG crystal structure (PDB ID 5F0A), and the human mTOR crystal structure (PDB ID 4JT5) were all prepared for docking using the Maestro protein preparation tool (Schrödinger Release 2021–3: Maestro, Schrödinger, LLC, New York, NY, 2021). Once prepared, a docking grid was created around the binding site using the GLIDE docking grid generation tool with a hydrogen bonding constraint set on the backbone amide of the critical hinge valine (*Pf*PI4Kβ, V1357; *Pv*PKG, V614; *Hu*mTOR, V2240). The structure of sapanisertib was then drawn using the Maestro 2D sketcher, after which it was prepared using the LigPrep tool at pH 7.0. Sapanisertib was then docked using GLIDE (55) at standard precision with the hydrogen bond constraint implemented. The output docked poses matched the expected pose of the analogous TORkinib compound bound to several kinases. Full residues within a 5.0-Å radius of the ligand were minimized using PRIME minimization in the function (56) and the OPLS4 force field.

Metabolomics

Parasite culturing for metabolic extractions—*Pf*3D7 parasites were cultured at 4% hematocrit under standard growth conditions and 6% O_2 and 5% CO_2. Sterile-filtered RPMI 1640 media (Gibco) supplemented with 25 mM Hepes, 23.8 mM $NaHCO_3$, 0.1 mM hypoxanthine, 0.25% (w/v) AlbuMAX II (Gibco), and gentamycin (50 μg/ml) was used as a standard culture medium with daily medium changes. Not including the cycle before metabolite extraction, parasites were synchronized two times by sorbitol lysis using a sterile-filtered 5% sorbitol solution in 1× phosphate-buffered saline (PBS) when parasites were mostly at the ring stage. The cultures were grown to ~10 to 15% parasitemia. Cultures were allowed to develop to the trophozoite stage and were then combined to

~10% hematocrit for magnetic purification using magnetic-activated cell sorting columns and Vario-Macs magnets. Magnetically separated infected RBCs (iRBCs) were centrifuged (Beckman Allegra 6R and 681-g GH-3.8/GH-3.8A Rotor) for 5 min at 1500 rpm and resuspended in RPMI media. The concentration of purified iRBCs was measured on a hemocytometer (Hausser Scientific). The cells were pelleted by centrifugation and diluted or concentrated to 1×10^8 cells/ml. Next, 1 ml of purified iRBCs was added in triplicate to wells with 4 ml of supplemented RPMI medium in six-well plates. The cultures had a 1-hour recovery period, after which cells were treated in triplicate at 10× IC_{50} compound concentration (or a control with no compound added) and incubated for 2.5 hours. A control treatment of atovaquone was also included at 10× IC_{50} (10 nM) to ensure reproducibility between treatment days. About 4 ml of media supernatant was then removed from each well, and the remaining 1 ml of suspended iRBCs was centrifuged (VWR Galaxy 5D microcentrifuge) for 0.5 min at 8500 rpm. The supernatant was aspirated, and pellets were washed carefully with 1 ml of ice cold 1× PBS and immediately centrifuged (VWR Galaxy 5D microcentrifuge) for 0.5 min at 8500 rpm. The 1× PBS supernatant was aspirated, and the pellet was quenched, and metabolites were extracted by the addition of 1 ml of 90% MeOH spiked with 0.5 μM [$^{13}C_4$,$^{15}N_1$]-labeled aspartate standard (Isotec Stable Isotopes) (57). Blank samples run in triplicate were composed of 1 ml of 90% MeOH spiked with 0.5 μM [$^{13}C_4$,$^{15}N_1$]-labeled aspartate standard. Samples were vortexed and centrifuged (Eppendorf Centrifuge 5424R and FA-45–24-11 Rotor) for 10 min at 4°C at 15,000 rpm. The supernatant was transferred into new 1.5-ml tubes, dried under nitrogen, and stored at −80°C before mass spectrometry analysis.

Extract sample preparation and mass spectrometry loading—Samples were thawed on ice and resuspended in ice-cold high-performance LC–grade water spiked with 1 μM chlorpropamide (Alfa Aesar) to a concentration of 1×10^6 cells/μl before loading on a Thermo Exactive Plus orbitrap liquid chromatography coupled mass spectrometer. Samples were vortexed and centrifuged (Eppendorf Centrifuge 5424R and FA-45–24-11 Rotor) for 10 min at 4°C at 15,000 rpm. The supernatant was then added to 800-μl CRIMP vials (Thermo Fisher Scientific) for mass spectrometry loading. As an additional quality control, pooled samples were constituted with 5 to 10 μl from each sample and run in triplicate on the mass spectrometer. Molecules in samples were separated using an XSelect HSS T3 2.5 μm C18 Waters column with a 25-min gradient of 3% aqueous methanol, 15 mM acetic acid, and 10 mM tributylamine as the ion pairing agent in negative ionization mode (negative electrospray ionization) and detected using the Thermo Exactive Plus orbitrap (58).

Analysis of mass spectrometry data—Raw data resulting from the mass spectrometry analysis were converted from .raw files to .mzXML files (59) for import into the el-MAVEN software package for peak picking (60). The datasets were normalized with the internal [$^{13}C_4$,$^{15}N_1$] aspartate-labeled standard. Fold change values were calculated by $\log_2\left(\frac{\text{drug}-\text{ treated line}}{\text{untreated line}}\right)$ and uploaded to Rstudio (www.rstudio.com/) using the packages Hyperspec and Suprahex (61). Fold change values were mapped onto a heatmap with 186 metabolites detected in all metabolomics extractions in Rstudio (www.rstudio.com/). Metabolic profiles were transferred to a two-dimensional hexagonal map with 113 metabolites separated into known metabolic pathways (17).

Statistics

In general, results were confirmed in $N \geq 2$ independent experiments with technical repeats as indicated in the figure legends. For the in vivo efficacy study, the sample size was small (two mice per dosing group). Where applicable, details of statistical analysis and the methods used are described elsewhere within the relevant Materials and Methods sections.

Supplementary Material

Refer to Web version on PubMed Central for supplementary material.

Acknowledgments:

We thank the Huck Institutes of Life Sciences Metabolomics Core Facility at Penn State University.

Funding:

This work was supported by the Future Leaders−African Independent Research (FLAIR) Fellowship Programme, a partnership between the African Academy of Sciences and the Royal Society funded by the UK Government's Global Challenges Research (to L.B.A.); the South African Medical Research Council (to K.C.); South African Research Chairs Initiative (SARChI) of the Department of Science and Innovation, administered through the South African National Research Foundation (SA NRF) (UID 64767 to K.C., UID 84627 to L.-M.B., and UID 64763 to L.L.K.); the NRF Communities of Practice grant from SARCHI (UID 110666 to L.-M.B., L.L.K., and K.C.); the Bill and Melinda Gates Foundation that funds the Malarial Drug Accelerator (MalDA) consortium (OPP1054480 to E.A.W., D.A.F., S.O., and M.L.; OPP1162467 to J.C.N.; and OPP1066878 to K.C.), and the Ruth L. Kirschstein Institutional National Research Award from the National Institute for General Medical Sciences T32 GM008666 (to M.R.L.).

REFERENCES AND NOTES

1. WHO, World Malaria Report 2021 (World Health Organization, 2021).
2. Fidock DA, Rosenthal PJ, Artemisinin resistance in Africa: How urgent is the threat? Med 2, 1287–1288 (2021). [PubMed: 35005674]
3. Duffey M, Blasco B, Burrows JN, Wells TNC, Fidock DA, Leroy D, Assessing risks of *Plasmodium falciparum* resistance to select next-generation antimalarials. Trends Parasitol 37, 709–721 (2021). [PubMed: 34001441]
4. Arendse LB, Wyllie S, Chibale K, Gilbert IH, Plasmodium kinases as potential drug targets for malaria: Challenges and opportunities. ACS Infect. Dis 7, 518–534 (2021). [PubMed: 33590753]
5. Voss MH, Gordon MS, Mita M, Rini B, Makker V, Macarulla T, Smith DC, Cervantes A, Puzanov I, Pili R, Wang D, Jalal S, Pant S, Patel MR, Neuwirth RL, Enke A, Shou Y, Sedarati F, Faller DV, Burris HA, Phase 1 study of mTORC1/2 inhibitor sapanisertib (TAK-228) in advanced solid tumours, with an expansion phase in renal, endometrial or bladder cancer. Br. J. Cancer 123, 1590–1598 (2020). [PubMed: 32913286]
6. Hassett MR, Roepe PD, PIK-ing new malaria chemotherapy. Trends Parasitol 34, 925–927 (2018). [PubMed: 29934102]
7. Bergamini G, Bell K, Shimamura S, Werner T, Cansfield A, Müller K, Perrin J, Rau C, Ellard K, Hopf C, Doce C, Leggate D, Mangano R, Mathieson T, O'Mahony A, Plavec I, Rharbaoui F, Reinhard F, Savitski MM, Ramsden N, Hirsch E, Drewes G, Rausch O, Bantscheff M, Neubauer G, A selective inhibitor reveals PI3Kγ dependence of TH17 cell differentiation. Nat. Chem. Biol 8, 576–582 (2012). [PubMed: 22544264]
8. Miranda-Saavedra D, Gabaldón T, Barton GJ, Langsley G, Doerig C, The kinomes of apicomplexan parasites. Microb. Infect 14, 796–810 (2012).
9. Balestra AC, Zeeshan M, Rea E, Pasquarello C, Brusini L, Mourier T, Subudhi AK, Klages N, Arboit P, Pandey R, Brady D, Vaughan S, Holder AA, Pain A, Ferguson DJ, Hainard A, Tewari R, Brochet M, A divergent cyclin/cyclin-dependent kinase complex controls the atypical replication

of a malaria parasite during gametogony and transmission. eLife 9, e56474 (2020). [PubMed: 32568069]

10. Fienberg S, Eyermann CJ, Arendse LB, Basarab GS, McPhail JA, Burke JE, Chibale K, Structural basis for inhibitor potency and selectivity of plasmodium falciparum phosphatidylinositol 4-kinase inhibitors. ACS Infect. Dis 6, 3048–3063 (2020). [PubMed: 32966036]
11. Hassett MR, thesis, Georgetown University, Washington, DC (2017).
12. Vanaerschot M, Murithi JM, Pasaje CFA, Ghidelli-Disse S, Dwomoh L, Bird M, Spottiswoode N, Mittal N, Arendse LB, Owen ES, Wicht KJ, Siciliano G, Bösche M, Yeo T, Kumar TRS, Mok S, Carpenter EF, Giddins MJ, Sanz O, Ottilie S, Alano P, Chibale K, Llinás M, Uhlemann A-C, Delves M, Tobin AB, Doerig C, Winzeler EA, Lee MCS, Niles JC, Fidock DA, Inhibition of resistance-refractory P *falciparum* kinase PKG delivers prophylactic, blood stage, and transmission-blocking antiplasmodial activity. Cell Chem. Biol 27, 806–816.e8 (2020). [PubMed: 32359426]
13. Ganesan SM, Falla A, Goldfless SJ, Nasamu AS, Niles JC, Synthetic RNA–protein modules integrated with native translation mechanisms to control gene expression in malaria parasites. Nat. Commun 7, 10727 (2016). [PubMed: 26925876]
14. Berndt A, Miller S, Williams O, Le DD, Houseman BT, Pacold JI, Gorrec F, Hon W-C, Ren P, Liu Y, Rommel C, Gaillard P, Rückle T, Schwarz MK, Shokat KM, Shaw JP, Williams RL, The p110δ structure: Mechanisms for selectivity and potency of new PI(3)K inhibitors. Nat. Chem. Biol 6, 117–124 (2010). [PubMed: 20081827]
15. El Bakkouri M, Kouidmi I, Wernimont AK, Amani M, Hutchinson A, Loppnau P, Kim JJ, Flueck C, Walker JR, Seitova A, Senisterra G, Kakihara Y, Kim C, Blackman MJ, Calmettes C, Baker DA, Hui R, Structures of the cGMP-dependent protein kinase in malaria parasites reveal a unique structural relay mechanism for activation. Proc. Natl. Acad. Sci. U.S.A 116, 14164–14173 (2019). [PubMed: 31239348]
16. Yang H, Rudge DG, Koos JD, Vaidialingam B, Yang HJ, Pavletich NP, mTOR kinase structure, mechanism and regulation. Nature 497, 217–223 (2013). [PubMed: 23636326]
17. Allman EL, Painter HJ, Samra J, Carrasquilla M, Llinás M, Metabolomic profiling of the malaria box reveals antimalarial target pathways. Antimicrob. Agents Chemother 60, 6635–6649 (2016). [PubMed: 27572391]
18. Kandepedu N, Cabrera DG, Eedubilli S, Taylor D, Brunschwig C, Gibhard L, Njoroge M, Lawrence N, Paquet T, Eyermann CJ, Spangenberg T, Basarab GS, Street LJ, Chibale K, Identification, characterization, and optimization of 2,8-disubstituted-1,5-naphthyridines as novel *Plasmodium falciparum* phosphatidylinositol-4-kinase inhibitors with in vivo efficacy in a humanized mouse model of malaria. J. Med. Chem 61, 5692–5703 (2018). [PubMed: 29889526]
19. Sternberg AR, Roepe PD, Heterologous expression, purification, and functional analysis of the *Plasmodium falciparum* phosphatidylinositol 4-kinase III β. Biochemistry 59, 2494–2506 (2020). [PubMed: 32543181]
20. Cheuka PM, Centani L, Arendse LB, Fienberg S, Wambua L, Renga SS, Dziwornu GA, New amidated 3,6-diphenylated imidazopyridazines with potent antiplasmodium activity are dual inhibitors of Plasmodium phosphatidylinositol-4-kinase and cGMP-dependent protein kinase. ACS Infect. Dis 7, 34–46 (2021). [PubMed: 33319990]
21. Paquet T, Le Manach C, Cabrera DG, Younis Y, Henrich PP, Abraham TS, Lee MCS, Basak R, Ghidelli-Disse S, Lafuente-Monasterio MJ, Bantscheff M, Ruecker A, Blagborough AM, Zakutansky SE, Zeeman A-M, White KL, Shackleford DM, Mannila J, Morizzi J, Scheurer C, Angulo-Barturen I, Martínez MS, Ferrer S, Sanz LM, Gamo FJ, Reader J, Botha M, Dechering KJ, Sauerwein RW, Tungtaeng A, Vanachayangkul P, Lim CS, Burrows J, Witty MJ, Marsh KC, Bodenreider C, Rochford R, Solapure SM, Jiménez-Díaz MB, Wittlin S, Charman SA, Donini C, Campo B, Birkholtz L-M, Hanson KK, Drewes G, Kocken CHM, Delves MJ, Leroy D, Fidock DA, Waterson D, Street LJ, Chibale K, Antimalarial efficacy of MMV390048, an inhibitor of *Plasmodium* phosphatidylinositol 4-kinase. Sci. Transl. Med 9, eaad9735 (2017). [PubMed: 28446690]
22. Krishnan K, Ziniel P, Li H, Huang X, Hupalo D, Gombakomba N, Guerrero SM, Dotrang T, Lu X, Caridha D, Sternberg AR, Hughes E, Sun W, Bargieri DY, Roepe PD, Sciotti RJ, Wilkerson MD, Dalgard CL, Tawa GJ, Wang AQ, Xu X, Zheng W, Sanderson PE, Huang W, Williamson KC,

Torin 2 derivative, NCATS-SM3710, has potent multistage antimalarial activity through inhibition of P. falciparum phosphatidylinositol 4-kinase (Pf PI4KIIIβ). ACS Pharmacol. Transl. Sci 3, 948–964 (2020). [PubMed: 33073193]

23. McNamara CW, Lee MCS, Lim CS, Lim SH, Roland J, Nagle A, Simon O, Yeung BKS, Chatterjee AK, McCormack SL, Manary MJ, Zeeman A-M, Dechering KJ, Kumar TRS, Henrich PP, Gagaring K, Ibanez M, Kato N, Kuhen KL, Fischli C, Rottmann M, Plouffe DM, Bursulaya B, Meister S, Rameh L, Trappe J, Haasen D, Timmerman M, Sauerwein RW, Suwanarusk R, Russell B, Renia L, Nosten F, Tully DC, Kocken CHM, Glynne RJ, Bodenreider C, Fidock DA, Diagana TT, Winzeler EA, Targeting Plasmodium PI(4)K to eliminate malaria. Nature 504, 248–253 (2013). [PubMed: 24284631]
24. Burke JE, Structural basis for regulation of phosphoinositide kinases and their involvement in human disease. Mol. Cell 71, 653–673 (2018). [PubMed: 30193094]
25. Zhang M, Wang C, Otto TD, Oberstaller J, Liao X, Adapa SR, Udenze K, Bronner IF, Casandra D, Mayho M, Brown J, Li S, Swanson J, Rayner JC, Jiang RHY, Adams JH, Uncovering the essential genes of the human malaria parasite *Plasmodium* falciparum by saturation mutagenesis. Science 360, eaap7847 (2018). [PubMed: 29724925]
26. Brunschwig C, Lawrence N, Taylor D, Abay E, Njoroge M, Basarab GS, Le Manach C, Paquet T, Cabrera DG, Nchinda AT, de Kock C, Wiesner L, Denti P, Waterson D, Blasco B, Leroy D, Witty MJ, Donini C, Duffy J, Wittlin S, White KL, Charman SA, Jiménez-Díaz MB, Angulo-Barturen I, Herreros E, Gamo FJ, Rochford R, Mancama D, Coetzer TL, van der Watt ME, Reader J, Birkholtz L-M, Marsh KC, Solapure SM, Burke JE, McPhail JA, Vanaerschot M, Fidock DA, Fish PV, Siegl P, Smith DA, Wirjanata G, Noviyanti R, Price RN, Marfurt J, Silue KD, Street LJ, Chibale K, UCT943, a next-generation *Plasmodium falciparum* PI4K inhibitor preclinical candidate for the treatment of malaria. Antimicrob. Agents Chemother 62, e00012–e18 (2018). [PubMed: 29941635]
27. Sinxadi P, Donini C, Johnstone H, Langdon G, Wiesner L, Allen E, Duparc S, Chalon S, McCarthy JS, Lorch U, Chibale K, Möhrle J, Barnes KI, Safety, tolerability, pharmacokinetics, and antimalarial activity of the novel *Plasmodium* phosphatidylinositol 4-kinase inhibitor MMV390048 in healthy volunteers. Antimicrob. Agents Chemother 64, e01896–19 (2020). [PubMed: 31932368]
28. Vaid A, Ranjan R, Smythe WA, Hoppe HC, Sharma P, PfPI3K, a phosphatidylinositol-3 kinase from *Plasmodium falciparum*, is exported to the host erythrocyte and is involved in hemoglobin trafficking. Blood 115, 2500–2507 (2010). [PubMed: 20093402]
29. Mbengue A, Bhattacharjee S, Pandharkar T, Liu H, Estiu G, Stahelin RV, Rizk SS, Njimoh DL, Ryan Y, Chotivanich K, Nguon C, Ghorbal M, Lopez-Rubio J-J, Pfrender M, Emrich S, Mohandas N, Dondorp AM, Wiest O, Haldar K, A molecular mechanism of artemisinin resistance in *Plasmodium falciparum* malaria. Nature 520, 683–687 (2015). [PubMed: 25874676]
30. Hassett MR, Sternberg AR, Riegel BE, Thomas CJ, Roepe PD, Heterologous expression, purification, and functional analysis of *Plasmodium falciparum* phosphatidylinositol 3′-kinase. Biochemistry 56, 4335–4345 (2017). [PubMed: 28719180]
31. Mott BT, Eastman RT, Guha R, Sherlach KS, Siriwardana A, Shinn P, McKnight C, Michael S, Lacerda-Queiroz N, Patel PR, Patel PR, Khine P, Sun H, Kasbekar M, Aghdam N, Fontaine SD, Liu D, Mierzwa T, Mathews-Griner LA, Ferrer M, Renslo AR, Inglese J, Yuan J, Roepe PD, Su X-Z, Thomas CJ, High-throughput matrix screening identifies synergistic and antagonistic antimalarial drug combinations. Sci. Rep 5, 13891 (2015). [PubMed: 26403635]
32. Iyengar K, thesis, Georgetown University, Washington, DC (2019).
33. Baker DA, Matralis AN, Osborne SA, Large JM, Penzo M, Targeting the malaria parasite cGMP-dependent protein kinase to develop new drugs. Front. Microbiol 11, 602803 (2020). [PubMed: 33391223]
34. Baker DA, Stewart LB, Large JM, Bowyer PW, Ansell KH, Jiménez-Díaz MB, El Bakkouri M, Birchall K, Dechering KJ, Bouloc NS, Coombs PJ, Whalley D, Harding DJ, Smiljanic-Hurley E, Wheldon MC, Walker EM, Dessens JT, Lafuente MJ, Sanz LM, Gamo F-J, Ferrer SB, Hui R, Bousema T, Angulo-Barturén I, Merritt AT, Croft SL, Gutteridge WE, Kettleborough CA, Osborne SA, A potent series targeting the malarial cGMP-dependent protein kinase clears infection and blocks transmission. Nat. Commun 8, 430 (2017). [PubMed: 28874661]

35. Matralis AN, Malik A, Penzo M, Moreno I, Almela MJ, Camino I, Crespo B, Saadeddin A, Ghidelli-Disse S, Rueda L, Calderon F, Osborne SA, Drewes G, Böesche M, Fernández-Álvaro E, Martin Hernando JI, Baker DA, Development of chemical entities endowed with potent fast-killing properties against *Plasmodium falciparum* malaria parasites. J. Med. Chem 62, 9217–9235 (2019). [PubMed: 31566384]
36. Kato N, Comer E, Sakata-Kato T, Sharma A, Sharma M, Maetani M, Bastien J, Brancucci NM, Bittker JA, Corey V, Clarke D, Derbyshire ER, Dornan GL, Duffy S, Eckley S, Itoe MA, Koolen KMJ, Lewis TA, Lui PS, Lukens AK, Lund E, March S, Meibalan E, Meier BC, McPhail JA, Mitasev B, Moss EL, Sayes M, Van Gessel Y, Wawer MJ, Yoshinaga T, Zeeman A-M, Avery VM, Bhatia SN, Burke JE, Catteruccia F, Clardy JC, Clemons PA, Dechering KJ, Duvall JR, Foley MA, Gusovsky F, Kocken CHM, Marti M, Morningstar ML, Munoz B, Neafsey DE, Sharma A, Winzeler EA, Wirth DF, Scherer CA, Schreiber SL, Diversity-oriented synthesis yields novel multistage antimalarial inhibitors. Nature 538, 344–349 (2016). [PubMed: 27602946]
37. Han J, Wang Y, mTORC1 signaling in hepatic lipid metabolism. Protein Cell 9, 145–151 (2018). [PubMed: 28434145]
38. Sofroniadou S, Goldsmith D, Mammalian target of rapamycin (mTOR) inhibitors. Drug Saf 34, 97–115 (2011). [PubMed: 21247219]
39. Rashidi S, Mansouri R, Ali-Hassanzadeh M, Mojtahedi Z, Shafiei R, Savardashtaki A, Hamidizadeh N, Karimazar M, Nguewa P, Manzano-Román R, The host mTOR pathway and parasitic diseases pathogenesis. Parasitol. Res 120, 1151–1166 (2021). [PubMed: 33534053]
40. Ren P, Liu Y, Wilson TE, Li L, Chan K, WO2010051042A1 (2013).
41. Adjalley SH, Johnston GL, Li T, Eastman RT, Ekland EH, Eappen AG, Richman A, Sim BKL, Lee MCS, Hoffman SL, Fidock DA, Quantitative assessment of *Plasmodium falciparum* sexual development reveals potent transmission-blocking activity by methylene blue. Proc. Natl. Acad. Sci. U.S.A 108, E1214–E1223 (2011). [PubMed: 22042867]
42. Reader J, van der Watt ME, Taylor D, Le Manach C, Mittal N, Ottilie S, Theron A, Moyo P, Erlank E, Nardini L, Venter N, Lauterbach S, Bezuidenhout B, Horatscheck A, van Heerden A, Spillman NJ, Cowell AN, Connacher J, Opperman D, Orchard LM, Llinás M, Istvan ES, Goldberg DE, Boyle GA, Calvo D, Mancama D, Coetzer TL, Winzeler EA, Duffy J, Koekemoer LL, Basarab G, Chibale K, Birkholtz L-M, Multistage and transmission-blocking targeted antimalarials discovered from the open-source MMV pandemic response box. Nat. Commun 12, 269 (2021). [PubMed: 33431834]
43. Hunt RH, Brooke BD, Pillay C, Koekemoer LL, Coetzee M, Laboratory selection for and characteristics of pyrethroid resistance in the malaria vector *Anopheles* funestus. Med. Vet. Entomol. 19, 271–275 (2005). [PubMed: 16134975]
44. Angulo-Barturen I, Jiménez-Díaz MB, Mulet T, Rullas J, Herreros E, Ferrer S, Jiménez E, Mendoza J Regadera, P. J. Rosenthal, I. Bathurst, D. L. Pompliano, F. G. de las Heras, D. Gargallo-Viola, A murine model of falciparum-malaria by in vivo selection of competent strains in non-myelodepleted mice engrafted with human erythrocytes. PLOS ONE 3, e2252 (2008). [PubMed: 18493601]
45. South African Bureau of Standards, “South African National Standard: The care and use of animals for scientific purposes” (SANS 10386:2008, SABS Standards Division, ed. 1, 2008).
46. Department of Health, “Ethics in health research: Principles, processes and structures” (Department of Health, Republic of South Africa, 2015).
47. Balestra AC, Koussis K, Klages N, Howell SA, Flynn HR, Bantscheff M, Pasquarello C, Perrin AJ, Brusini L, Arboit P, Sanz O, Castaño LP, Withers-Martinez C, Hainard A, Ghidelli-Disse S, Snijders AP, Baker DA, Blackman MJ, Brochet M, $Ca2^{+}$ signals critical for egress and gametogenesis in malaria parasites depend on a multipass membrane protein that interacts with PKG. Sci. Adv 7, eabe5396 (2021). [PubMed: 33762339]
48. Bantscheff M, Hopf C, Savitski MM, Dittmann A, Grandi P, Michon A-M, Schlegl J, Abraham Y, Becher I, Bergamini G, Boesche M, Delling M, Dümpelfeld B, Eberhard D, Huthmacher C, Mathieson T, Poeckel D, Reader V, Strunk K, Sweetman G, Kruse U, Neubauer G, Ramsden NG, Drewes G, Chemoproteomics profiling of HDAC inhibitors reveals selective targeting of HDAC complexes. Nat. Biotechnol 29, 255–265 (2011). [PubMed: 21258344]

49. Werner T, Sweetman G, Savitski MF, Mathieson T, Bantscheff M, Savitski MM, Ion coalescence of neutron encoded TMT 10-plex reporter ions. Anal. Chem 86, 3594–3601 (2014). [PubMed: 24579773]
50. Moggridge S, Sorensen PH, Morin GB, Hughes CS, Extending the compatibility of the SP3 paramagnetic bead processing approach for proteomics. J. Proteome Res 17, 1730–1740 (2018). [PubMed: 29565595]
51. Sridharan S, Kurzawa N, Werner T, Günthner I, Helm D, Huber W, Bantscheff M, Savitski MM, Proteome-wide solubility and thermal stability profiling reveals distinct regulatory roles for ATP. Nat. Commun 10, 1155 (2019). [PubMed: 30858367]
52. Penzo M, de Las Heras-Dueña L, Mata-Cantero L, Diaz-Hernandez B, Vazquez-Muñiz M-J, Ghidelli-Disse S, Drewes G, Fernandez-Alvaro E, Baker DA, High-throughput screening of the *Plasmodium falciparum* cGMP-dependent protein kinase identified a thiazole scaffold which kills erythrocytic and sexual stage parasites. Sci. Rep 9, 1–13 (2019). [PubMed: 30626917]
53. Murithi JM, Owen ES, Istvan ES, Lee MCS, Ottilie S, Chibale K, Goldberg DE, Winzeler EA, Llinás M, Fidock DA, Vanaerschot M, Combining stage specificity and metabolomic profiling to advance antimalarial drug discovery. Cell Chem. Biol 27, 158–171.e3 (2020). [PubMed: 31813848]
54. Cingolani P, Platts A, Wang LL, Coon M, Nguyen T, Wang L, Land SJ, Lu X, Ruden DM, A program for annotating and predicting the effects of single nucleotide polymorphisms, SnpEff. Fly 6, 80–92 (2012). [PubMed: 22728672]
55. Friesner RA, Banks JL, Murphy RB, Halgren TA, Klicic JJ, Mainz DT, Repasky MP, Knoll EH, Shelley M, Perry JK, Shaw DE, Francis P, Shenkin PS, Glide: A new approach for rapid, accurate docking and scoring. 1. Method and assessment of docking accuracy. J. Med. Chem 47, 1739–1749 (2004). [PubMed: 15027865]
56. Jacobson MP, Friesner RA, Xiang Z, Honig B, On the role of the crystal environment in determining protein side-chain conformations. J. Mol. Biol 320, 597–608 (2002). [PubMed: 12096912]
57. Olszewski KL, Llinás M, Extraction of hydrophilic metabolites from *Plasmodium falciparum*-infected erythrocytes for metabolomic analysis. Methods Mol. Biol 923, 259–266 (2013). [PubMed: 22990783]
58. Lu W, Clasquin MF, Melamud E, Amador-Noguez D, Caudy AA, Rabinowitz JD, Metabolomic analysis via reversed-phase ion-pairing liquid chromatography coupled to a stand alone orbitrap mass spectrometer. Anal. Chem 82, 3212–3221 (2010). [PubMed: 20349993]
59. Keller A, Eng J, Zhang N, Li XJ, Aebersold R, A uniform proteomics MS/MS analysis platform utilizing open XML file formats. Mol. Syst. Biol 1, 2005.0017 (2005).
60. Agrawal S, Kumar S, Sehgal R, George S, Gupta R, Poddar S, Jha A, Pathak S, El-MAVEN: A fast, robust, and user-friendly mass spectrometry data processing engine for metabolomics. Methods Mol. Biol 1978, 301–321 (2019). [PubMed: 31119671]
61. Fang H, Gough J, supraHex: An R/Bioconductor package for tabular omics data analysis using a supra-hexagonal map. Biochem. Biophys. Res. Commun 443, 285–289 (2014). [PubMed: 24309102]
62. Sud M, Fahy E, Cotter D, Azam K, Vadivelu I, Burant C, Edison A, Fiehn O, Higashi R, Nair KS, Sumner S, Subramaniam S, Metabolomics Workbench: An international repository for metabolomics data and metadata, metabolite standards, protocols, tutorials and training, and analysis tools. Nucleic Acids Res 44, D463–D470 (2016). [PubMed: 26467476]

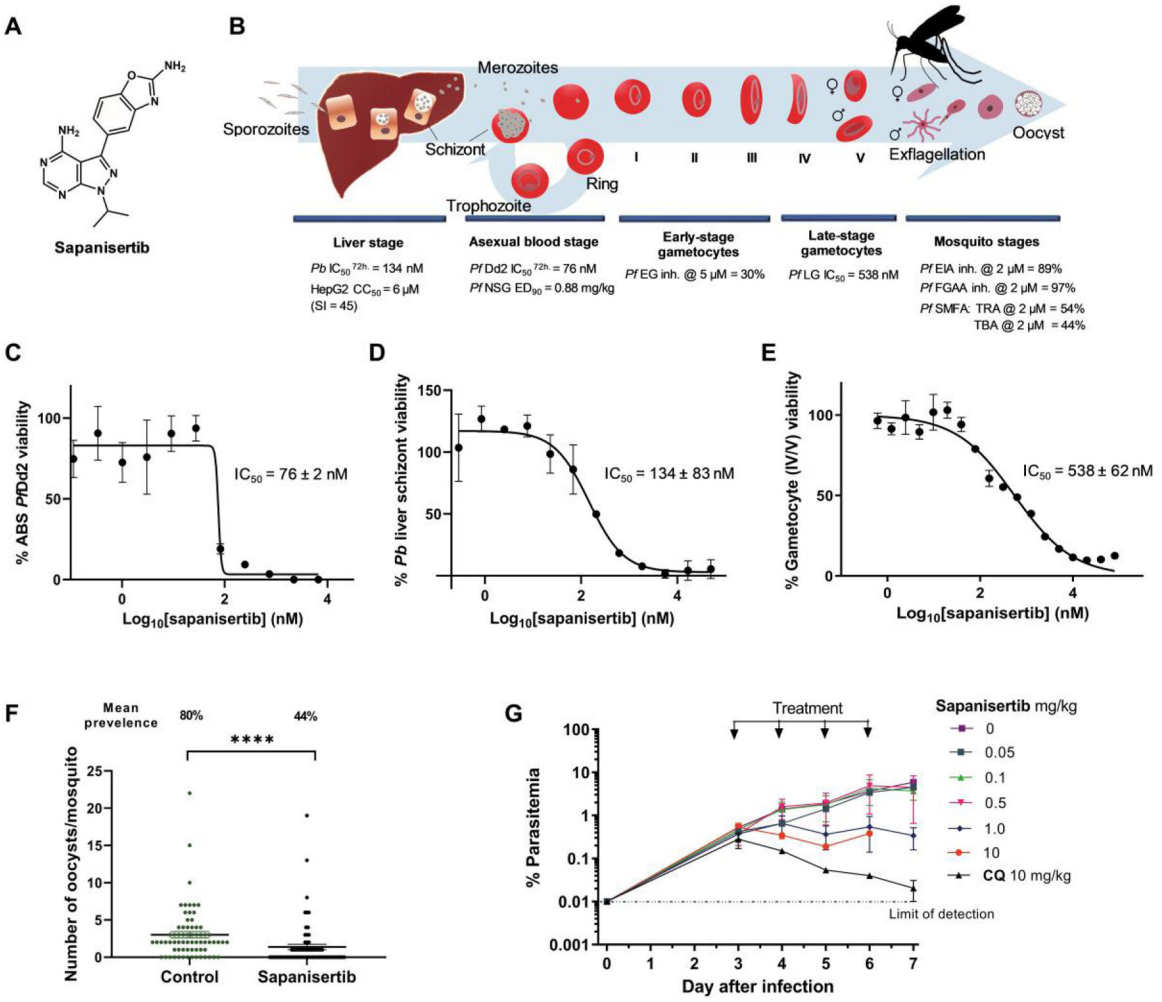

Fig. 1. Antiplasmodial activity of sapanisertib across the parasite life cycle.

(**A**) Structure of pyrazolopyrimidine sapanisertib. (**B**) Schematic overview of *Plasmodium* life cycle and sapanisertib antiplasmodial activity based on stage-specific experimental models. (**C**) Antiplasmodial activity of sapanisertib in an in vitro *P. falciparum* Dd2 asexual blood stage (ABS) assay. Dose-response curve generated from two independent biological repeats, with technical duplicates (mean IC_{50} value ± SD). (**D**) Prophylactic antiplasmodial activity of sapanisertib in an in vitro *P. berghei* ANKA liver stage assay. Dose-response curve generated from two independent biological repeats, with technical quadruplicates (mean IC_{50} value ± SD). (**E**) Effect of sapanisertib on late-stage (IV/V) gametocytes determined by measuring luminescence of recombinant *P. falciparum* parasites expressing luciferase (mean ± SEM based on three independent biological repeats, with technical triplicates). (**F**) Number of oocysts in the midgut of mosquitoes and prevalence of infected mosquitoes after feeding on stage V gametocytes treated with either sapanisertib ($n = 71$) or vehicle (control, $n = 69$) in the SMFA (combined data from four biological repeats). Each dot represents the number of oocysts in a single mosquito midgut. The Mann-Whitney U test was used to compare the statistical significance between the sapanisertib treatment and the vehicle control (****$P < 0.0001$). Mean prevalence refers to the percentage of infected

mosquitoes (containing ≥1 oocyst per midgut) in each group. (**G**) Oral in vivo therapeutic efficacy of sapanisertib in an NSG mouse model of *Pf*3D7 infection. Parasitemia is shown as a function of time after once-daily dosing of sapanisertib for 4 days [$N = 2$ per dose level, except for 0.05 mg/kg group where $N = 1$, error bars represent ± SEM]. Dosing commenced on day 3 after infection. Chloroquine (CQ; 10 mg/kg) was included as a control. *Pb, P. berghei*; *Pf, P. falciparum*; IC_{50}, 50% inhibitory concentration; CC_{50}, 50% cytotoxic concentration; SI, selectivity index (HepG2 CC_{50}/*Pb* IC_{50}); NSG, NOD-*scid IL-2R*γ^{null}; EG, early-stage gametocytes (>95% stages II/III); LG, late-stage gametocytes (>90% stage IV/V); EIA, exflagellation inhibition assay; FGAA, female gamete activation assay; SMFA, standard membrane feeding assay; TRA, transmission-reducing activity (% inhibition in mean oocyst count); TBA, transmission-blocking activity (% inhibition in prevalence of infected mosquitoes). Data points for replicates are included in data file S1.

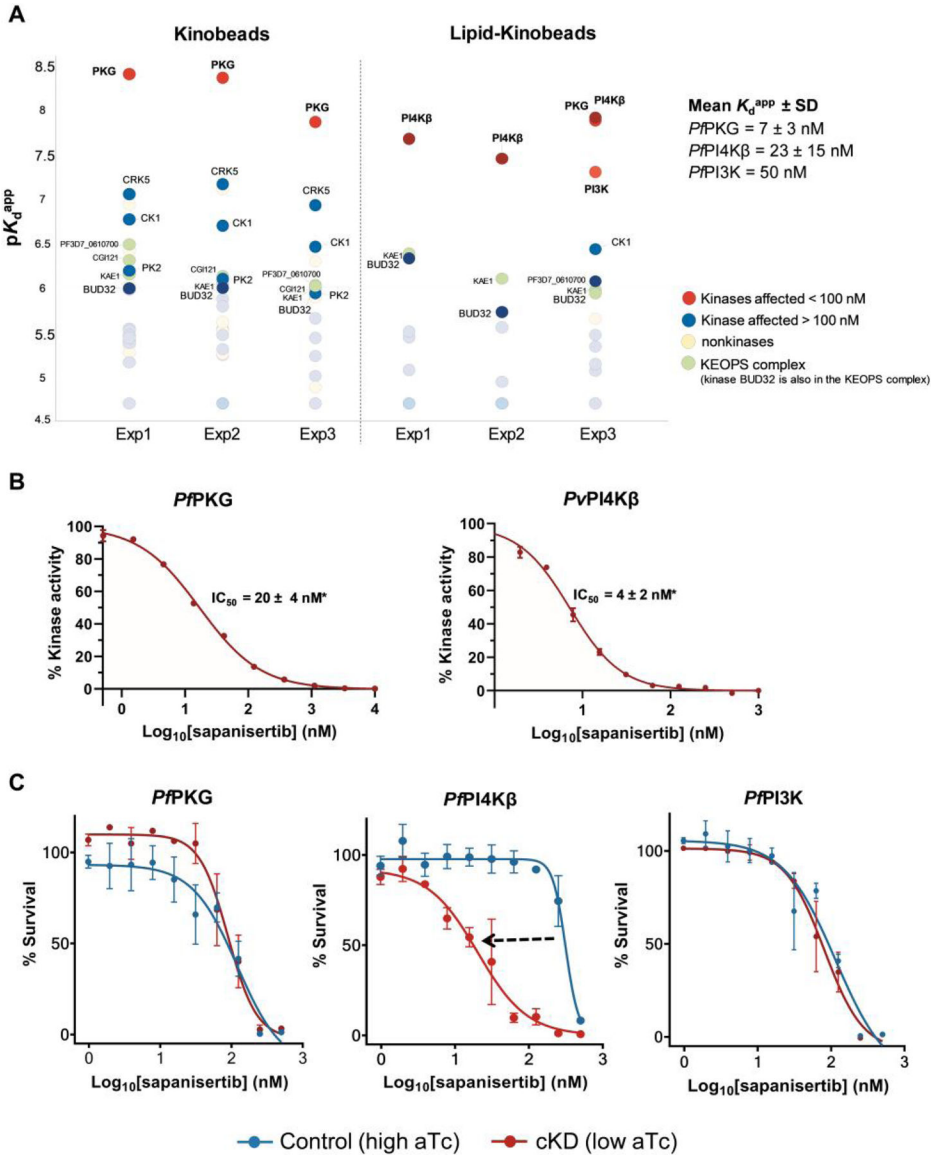

Fig. 2. Identification and validation of the Plasmodium kinase targets of sapanisertib.

(**A**) Chemoproteomic studies were carried out using Kinobead technology to identify putative kinase targets from *P. falciparum* ABS extracts. This approach uses sets of broad-spectrum ATP-competitive protein and lipid kinase inhibitors covalently immobilized to Sepharose beads to affinity-capture kinases from cell extracts. The K_d^{app} values for *P. falciparum* proteins that were competitively inhibited from binding to the beads by sapanisertib in a dose-dependent manner were determined on the basis of three independent experiments (see data file S2 for full names and PlasmoDB identifiers). (**B**) Inhibition of recombinant *Pf*PKG and *Pv*PI4Kβ by sapanisertib. A representative dose-response curve is shown for each enzyme. Error bars represent ±SD for technical duplicates. *Mean IC_{50} values ± SD were calculated on the basis of $N \geq 3$ independent experiments, each with technical duplicates (data file S3). Assays were carried out in the presence of 10 μM ATP, and enzyme activity was measured by quantifying the amount of ADP produced during

the kinase reaction using the ADP-Glo Kinase Assay. (**C**) Effect of conditional knockdown (cKD) of PKG, PI4Kβ or PI3K on parasite sensitivity to sapanisertib, relative to control conditions in the presence of high aTc. Representative dose-response curves are shown for each cKD parasite line. Error bars represent ± SD for technical duplicates. Results were confirmed in $N \geq 3$ independent experiments (data file S4).

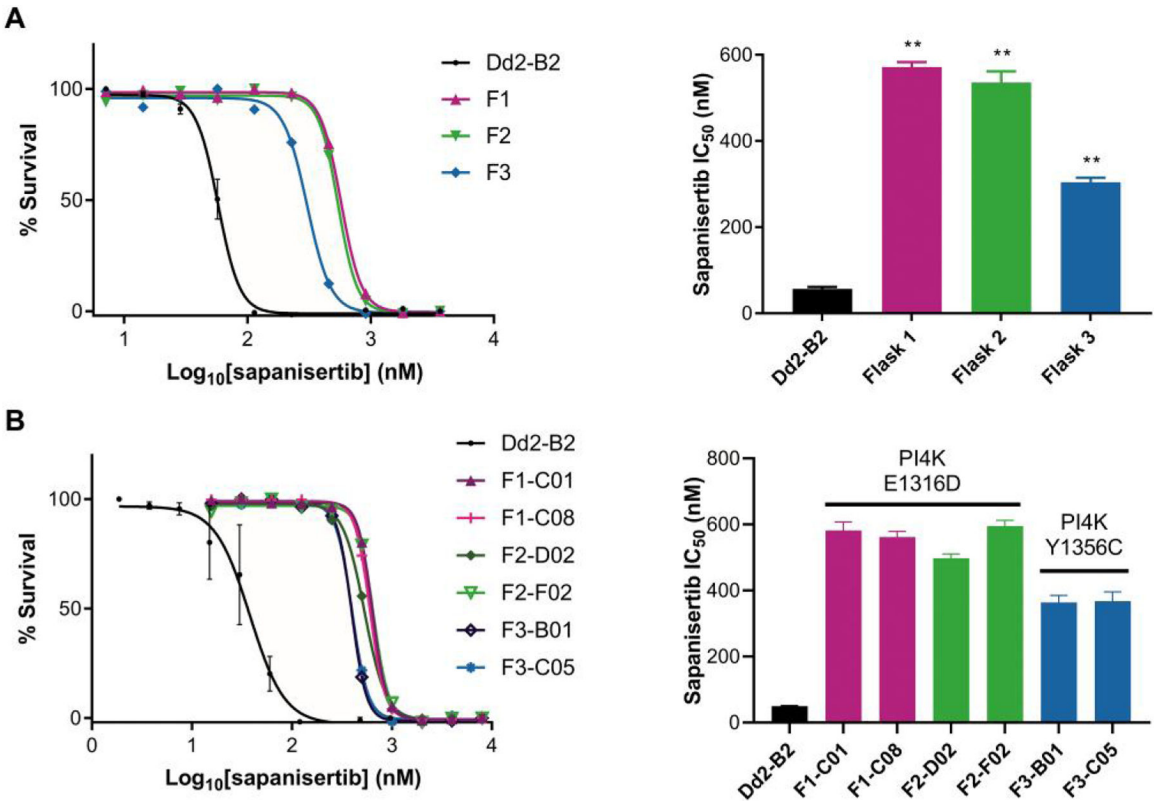

Fig. 3. In vitro selections identify mutations in PI4Kβ as sapanisertib-resistance mediators in cultured P. falciparum ABS parasites.

(**A**) Resistant bulk-culture parasite susceptibility to sapanisertib from three independent flasks (F1, F2, and F3) obtained after 16 days of continuous drug exposure at 5× 72-hour IC_{50}. Mean *P. falciparum* ABS IC_{50} values, with error bars indicating SEM, were determined from five independent assays with technical duplicates, $^{**}P < 0.01$. (**B**) Sapanisertib susceptibility profile of gene-edited resistant clones containing mutations in the kinase domain of PI4Kβ as confirmed by whole-genome sequencing (data file S5). Means ± SEM IC_{50} values were determined from three independent experiments with technical duplicates.

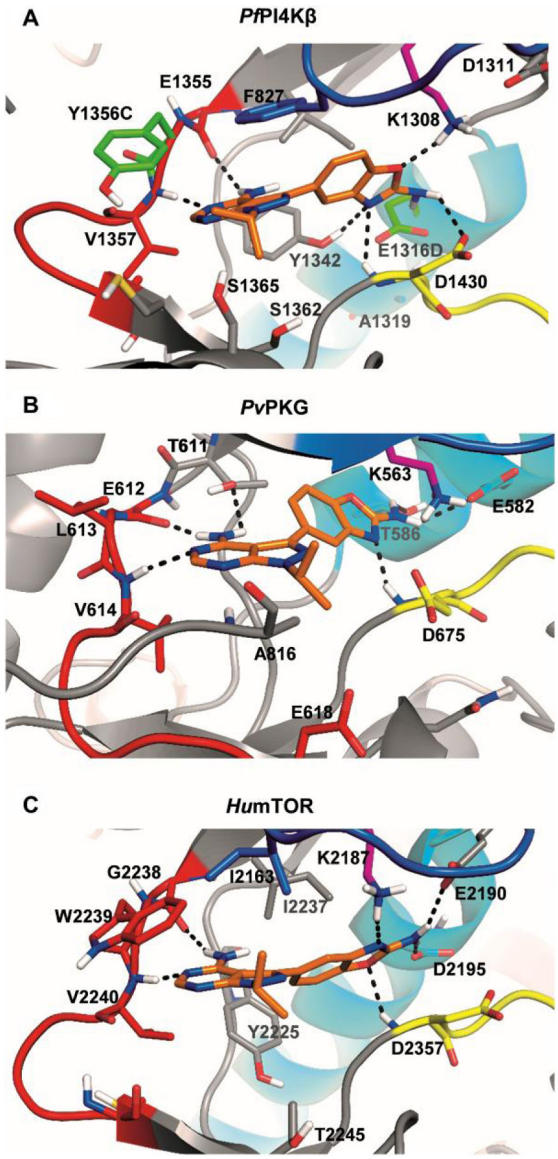

Fig. 4. In silico modeling predicts protein-inhibitor interactions in ATP-binding sites of kinase targets.

Sapanisertib (orange) docked into ATP-binding site of (**A**) *Pf*PI4Kβ homology (10), (**B**) *Pv*PKG crystal structure (PDB 5F0A), and (**C**) human mTOR crystal structure (PDB 4JT5). Conserved features of the kinase domain are shown as follows: hinge region in red; P-loop in blue; catalytic lysine residue within β sheet-3 in magenta; catalytic αC helix in cyan; DFG motif within activation segment in yellow. Selected main chains and side chains of key residues are shown as sticks with hydrogen bonds between sapanisertib and protein residues displayed as black dashed lines. *Pf*PI4Kβ residues Y1356 and E1316 that were mutated in laboratory-generated sapanisertib-resistant lines are shown in green.

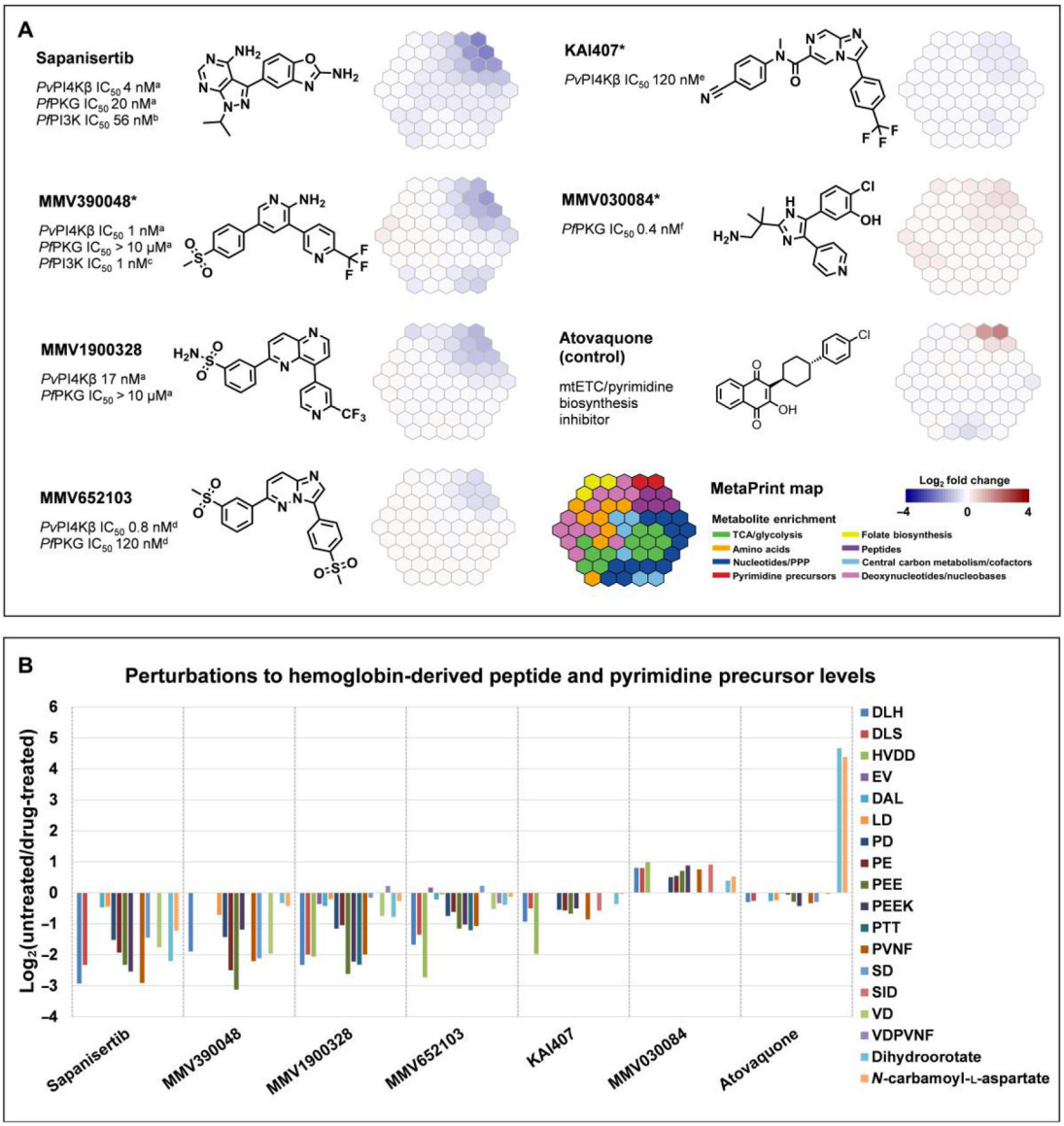

Fig. 5. Metabolomic fingerprint analysis after treatment of P. falciparum trophozoites with kinase inhibitors.

(**A**) Data are presented using two-dimensional hexagonal maps (metaprints) wherein 113 targeted metabolites are represented as metabolite clusters, separated into eight known metabolic pathways (17). Metaprints were assembled on the basis of the metabolomic perturbation profiles for each compound, as determined from the $\log_2$-fold changes in values of metabolites after drug treatment relative to an untreated (no-drug) control (data file S6). Atovaquone was included at 10 × IC_{50} (10 nM) as a control to ensure reproducibility between treatment days. *Metabolomics data shown for MMV390048 (17), KAI407 (53), and MMV030084 (12) have previously been published. Chemical structures and reported in vitro biochemical data for *Pv*PI4Kβ, *Pf*PKG, and *Pf*PI3K are also shown ([a]data were generated using methods described in this study; [b]Hassett *et al.* (11); [c]Sternberg *et al.* (19); [d]Cheuka *et al.* (20); [e]McNamara *et al.* (23); [f]Vanaerschot *et al.* (12). mtETC, mitochondrial electron transport chain; TCA, tricarboxylic acid cycle; PPP, pentose phosphate pathway.

(**B**) Graph illustrates the $\log_2$-fold changes in values of hemoglobin-derived peptide and pyrimidine precursor levels relative to a no-drug control for each inhibitor tested.